AN ANALYTICAL INVESTIGATION OF THE EFFECT OF BLADE PROFILE VARIATIONS ON THE EROSION OF COAL-FIRED TURBINE BLADES

by

Jack Allan Kinback

Thesis submitted to the Graduate Faculty of the

Virginia Polytechnic Institute and State University

in partial fulfillment of the requirements of the degree of

MASTER OF SCIENCE

in

Mechanical Engineering

APPROVED:

H. L. Moses

W. F. O'Brien, Jr.

N. S. Eiss

August, 1978

Blacksburg, Virginia 24061

II. ACKNOWLEDGEMENTS

The author would like to express sincere appreciation to the members of his graduate advisory committee: Professors N. S. Eiss, H. L. Moses, Chairman, and W. F. O'Brien, Jr. The author also thanks for his invaluable assistance throughout the investigation.

The author is grateful to the Mechanical Engineering Department, whose fellowship funds made his graduate work possible.

III. TABLE OF CONTENTS

IV. List of Figures

V. LIST OF TABLES

VI. LIST OF SYMBOLS

Roman Symbols

A	coefficient of velocity gradient equation
A_o, A_1, A_2, A_3, A_4	constants of profile-thickness form equation
B	coefficient of velocity gradient equation
B_0, B_1, B_2	constants of mean line equation
C	absolute gas velocity
C_1, C_3	absolute gas velocity at stator inlet and rotor exit
C_a	absolute axial gas velocity
C_d	drag coefficient
C_p	constant pressure specific heat
d_p	particle diameter
E	specific erosion rate
$f\ (R_e)$	a function of Reynolds number
$\vec{F}_D$	drag force
h	stream channel thickness
K_1, K_2	amplitudes of erosion for brittle and ductile modes
k	specific heat ratio
M	maximum ordinate of thickness form
M_1	mass of impacting particle
m	meridional streamline distance
m_1, m_2	velocity exponents for brittle and ductile modes of erosion

m_o	combined velocity exponent of erosion
P	position of maximum ordinate
r	radial coordinate
r_L	leading edge radius of airfoil
R_1, R_2	leading edge radius of Westinghouse Model 501B stator and rotor
R_e	Reynolds number
S	volume of material eroded per particle impact
T	gas temperature
T_1, T_2, T_3	static temperature at stage inlet, stator exit, and rotor exit
T_{01}, T_{02}, T_{03}	total temperature at stage inlet, stator exit, and rotor exit
T_i	inlet stagnation temperature
t	maximum thickness of airfoil
U	blade speed
V_2, V_3	relative gas velocity at rotor inlet and exit
V_G	gas velocity
V_p	particle velocity
V_{p_1}, V_{p_2}	particle velocity before and after impact
$V_{p_{el}}$	particle velocity corresponding to elastic deformation
$V_{p_{n1}}$, $V_{p_{n2}}$	particle velocity component in the direction normal to the surface before and after impact
$V_{p_{t1}}$, $V_{p_{t2}}$	particle velocity component in the direction tangential to the surface before and after impact
$V_{p_{tr}}$	residual horizontal velocity component following impact

V_x, V_m, V_r, V_θ	gas velocity components in the x, m, r, and θ directions
W	relative gas velocity
W_m, W_θ	relative gas velocity in the m and θ directions
W_s	stage work of turbine
w	blade-to-blade mass flow rate
x	axial coordinate
x_A, y_A	axial flow turbine coordinate system, Figure 3
$\dot{x}_p$, $\dot{r}_p$, $\dot{\theta}_p$	particle velocity components in the x, r, and θ directions
$\ddot{x}_p$, $\ddot{r}_p$, $\ddot{\theta}_p$	particle acceleration components in the x, r, and θ directions
y	blade profile ordinate, Figure 2
y_c	ordinate of mean camber line
y_t	blade profile - thickness ordinate

Greek Symbols

α	stagger angle
α_2, α_3	absolute angle of gas flow at rotor inlet and exit
β	angle between the velocity vector and meridional plane
β_{max}	impact angle for maximum erosion
β_0	reference angle
β_1, β_2	particle incidence angle before and after impact
β_1', β_2'	inlet and exit blade angle, Figure 3
β_3	relative angle of gas flow at rotor exit
Δh_{static}	static enthalpy drop across stage

ε	threshold energy for brittle erosion
ε_i	inlet prerotation
γ_1, γ_2	inlet and exit blade angles, Figure 2
θ_1, θ_2	circumferential coordinate at lower and upper boundaries
θ_T	angle between tangent to mean line and x-axis
λ	angle between turbine axis and streamline direction
μ_g	absolute gas viscosity
ρ_g	gas density
ρ_i	inlet gas stagnation density
ρ_p	particle density
ϕ	threshold energy for ductile erosion
ψ	stream function
ω	blade rotational speed

Subscripts

u	blade profile upper surface
1	blade profile lower surface

VII. INTRODUCTION

Shortly after World War II reliable industrial gas turbines were developed, aided by the technology and materials of the aircraft jet engine. These turbines were capable of burning only relatively clean fuels, particularly oil and natural gas. Since the early 1970's, the increasing price of these fuels has led government and industry to seek alternative energy sources for the gas turbine. One possibility is the burning of crushed coal or a coal derived fuel in an open cycle gas turbine. These fuels contain mineral constituents, however, which when carried over in the combustion gases will cause erosion, deposition, and corrosion of the turbine blades.

In an effort to determine the tolerance of industrial gas turbines to erosion by coal ash particles, Menguturk and Sverdrup (1)* developed a computer program simulating the erosion of axial flow turbine blades. Their work was primarily aimed at determining the allowable limits of particle size and concentration in a commercially operable machine.

This investigation utilizes the computer program of Menguturk and Sverdrup to determine the effect of certain blade profile variations on turbine blade erosion. This will provide design criteria for the development of erosion resistant turbine blades.

---

*Numbers in parentheses refer to references listed at the end of the thesis.

VIII. REVIEW OF LITERATURE

Experimental Investigations

Research efforts towards the development of a coal-fired gas turbine were begun in the United States in 1944 by the Locomotive Development Committee (L.D.C.) of Bituminous Coal Research, Inc. The L.D.C. operated a coal-fired Houdry 5-stage reaction turbine for more than 1,000 hours at their Dunkirk, New York Laboratories prior to 1951. Between 1951 and 1958 an Allis-Chalmers 6-stage locomotive gas turbine was operated for more than 4,000 hours. The L.D.C. program was terminated in 1959 when no practical method of further eliminating turbine blade erosion could be found.

The United States Bureau of Mines continued the investigation initiated by the L.D.C., transferring the project to Morgantown, West Virginia. The Bureau of Mines investigation continued until the late 1960's. New blades were designed for the turbine and almost 2,000 hours of operation completed. The new blade design showed improved resistance to erosion over the L.D.C. blades.

The original Houdry turbine of the L.D.C. was operated in four 250-hour tests during 1950 and 1951. Descriptions of the apparatus and the results of these tests are given in references 2 through 6.

In 1951, a 3168 KW Allis-Chalmers prototype locomotive gas turbine was installed at the L.D.C. facility (7). The turbine was operated for 757 hours in early 1952. Erosion occurred at the trailing edge of the first five rows of rotor and stator blades,

becoming progressively less toward the low pressure end of the turbine. No significant ash deposition occurred (8, 9, 10, 11, 12).

After the 757-hour test, the turbine was rebladed. The first four rows of rotor blades were replaced with blades of 19-9DL steel. Stator blades of S-590 alloy were installed. The reconditioned turbine was operated for 1,721 hours.

During the 1721-hour test, semi-circular notches were cut in the rotor blades near the blade root. Notches developed in the trailing edge of some of the blades causing cracks to form in 27 due to stress concentrations (13, 14, 15).

The turbine was again reconditioned after the 1721-hour test. This included the introduction of a deflector ring in front of the first stage stator blades and the installation of skimmers to remove ash concentrations. Rotor blades of HS-31 and GMR-235 alloy were installed. The turbine was operated for another 1,103 hours (16).

During this test, the second, third, and fourth stage rotor blades were again seriously eroded at the leading edge near the blade root. Notches were also cut at the base of the leading edge of the stator blades.

At this point the Bureau of Mines obtained the L.D.C. turbine and associated equipment. It contracted the Gas Turbine Division of General Electric Company to evaluate the L.D.C. operations and design new blades for the turbine (17).

Since the primary gas flow through the turbine follows a helical path, the ash particles would be expected to concentrate at the

outer sidewall. The L.D.C. tests showed, however, that secondary flows concentrate significant amounts of ash near the rotor drum (18). It was desired, therefore, to redesign the blading so as to concentrate the ash at the turbine outer sidewall, away from the critical rotor blade roots.

The new blade design presented by G.E. thickened the trailing edge of the rotor blades to encourage radially outward secondary flows. The trailing edge of the stators was thinned to inhibit radially inward flows. An annulus was created after the first stator blade row to provide space for the ash to centrifuge to the outer sidewall. Titanium carbide wear strips were inserted at the rotor and stator blade roots where erosion had been maximum in the L.D.C. tests.

The Bureau of Mines conducted two tests with the new blade design totaling 1,963 hours (19). Heavy ash deposits in the first stator row after 878 hours caused compressor surge and necessitated the termination of the first test (21, 21).

After cleaning and reconditioning, a second test of 1,085 hours was conducted. During this test, ash buildup in the first stator row was not as heavy. Inspection of the turbine showed that the stator blades of rows two through four were eroded seriously at the blade root. The trailing edge of these blades was also heavily eroded. The rotor blades showed little damage. The estimated blade life at the conclusion of these tests was 20,000-30,000 hours for the rotor and 5,000-7,500 hours for the stator (19). No further tests were made

with the Allis-Chalmers turbine.

Despite the limited success of the Bureau of Mines and the L.D.C., a coal-burning gas turbine locomotive was designed and built by Union Pacific Railroad and the American Locomotive Company (22, 23). Beginning in October 1962, this locomotive was tested for nearly a year. In its initial operation, power fell off badly in 200 hours. Improvements in the cyclone separating system increased the operating time to only 400 hours before severe power loss occurred (24).

Another of the more successful coal-burning gas turbine development efforts took place at the Aeronautical Research Laboratories in Melbourne, Australia. The core of this program entailed the operation of a Ruston and Hornsby type "TA" open cycle gas turbine (25). Trial runs of 200 hours were undertaken with brown coal in 1963. Turbine blade erosion similar to that experienced by the L.D.C. occurred.

At this point, the turbine was redesigned with lower gas velocities and blades of greater trailing edge thickness. 125 hours of operation of the redesigned turbine were completed in 1970 (26). Inspection of the turbine blades showed that erosion rates had been reduced by a factor of 10 to 20. Estimated blade life was in the range of 25,000-50,000 hours (26). It was concluded that blade life of this order was adequate for commercial needs.

Ash deposits in the Ruston and Hornsby turbine were controlled by intermittent water injection into the combustion gases (27). If water injection proved inadequate, small quantities of a substance called Kaolin were found to remove even the hardest ash deposits.

McGill University in Canada began a coal-fired gas turbine development program in 1949 (28). The program concentrated on an exhaust heated cycle, the advantage being that only heated air passed through the turbine. Ash buildup in the furnace and heat exchanger were considered the major problems when the project was discontinued in the late 1950's (29).

Less extensive development efforts were made by Brown Boveri of Switzerland and the Ministry of Fuel and Power, Great Britain (30, 26). Other European efforts include programs by Escher Wyss, C. A. Parsons and Company, and Ruston and Hornsby (26).

Analytical Investigations

The first mathematical model of erosion was developed by Finnie as a result of his studies of erosive particle speeds using high-speed photographic techniques (31, 32). Finnie's original equations were modified by Bitter to include two types of wear, these being wear due to repeated deformation and cutting wear (33, 34). Neilson and Gilchrist further modified Bitter's equations defining total erosion as a combination of the brittle and ductile components (35).

Head and Harr (36) concluded that the models developed by Bitter and Finnie were of little value when applied to erosion caused by nonhomogeneous contaminants. These authors chose to describe their experimental data in a statistical manner, using the Buckingham Pi Theorem.

Grant (37) derived a mathematical model of erosion following a procedure similar to Bitter's. The necessary equation constants were experimentally obtained by Grant and Tabakoff for the erosion of 2024 aluminum alloy.

The erosion of turbomachinery components due to particulates in the gas stream has been investigated extensively by Tabakoff (38, 39, 40, 41, 42). Hussein and Tabakoff developed a computer program to predict particle trajectories in turbine blade cascades (43, 44). This work was extended to radial inflow turbines by Clevenger and Tabakoff (45). The erosion model of Grant was incorporated into these particle trajectory programs to predict the erosion due to solid particles ingested into rotating machinery (46, 47).

Concurrently, Menguturk and Sverdrup of Westinghouse Electric Corporation developed a similar particle trajectory model for axial flow turbines (1). The erosion model of Bitter was incorporated into their computer program. Ulke (48) extended their work to include end wall boundary layers, radial flows, and blade wakes. Dubberley (49) used the computer program of Menguturk and Sverdrup to determine the effect of blade profile variations on the total erosion of axial flow turbine blades. The blade profile variations made in Dubberley's study are subject to criticism because of their arbitrariness.

IX. ANALYSIS

The purpose of this investigation is to determine the effect of certain blade profile variations on the erosion of an axial flow gas turbine. Three computer programs are used to accomplish this objective. The first program creates blade profiles for the desired blade parameters. The second program, a modification of the Katsanis blade-to-blade potential solution (50), determines the flow field for a turbine passage bounded by the above blade profiles. Finally, the particle trajectory model developed by Menguturk and Sverdrup (1) is used to determine the blade erosion corresponding to each blade passage configuration.

The theoretical development of each computer program is outlined below. A method of varying degree of reaction is also summarized.

Blade Profile Model

A conventional approach to turbine blade design is to combine a profile-thickness form, which is known to be efficient, with a mean line form. This approach is summarized in references 51 through 55. The blade profile model used in this investigation follows the method of reference 55, NACA TR 460. The model is developed so that the blade parameters of inlet angle, exit angle, thickness, chord length, stagger angle, and leading edge radius can be varied as desired.

A well-known class of airfoils including the Göttingen 398 and the Clark Y are known to be efficient and are nearly alike when their

camber is removed and they are reduced to the same maximum thickness. An equation of the form,

$$\pm y = A_o\sqrt{x} + A_1 x + A_2 x^2 + A_3 x^3 + A_4 x^4 \tag{1}$$

with the conditions

1) Maximum ordinate 0.1 at 0.3 chord

$x = 0.3 \qquad y = 0.1$

$\frac{dy}{dx} = 0$

2) Ordinate at trailing edge

$x = 1 \qquad y = 0.002$

3) Trailing-edge angle

$x = 1 \qquad \frac{dy}{dx} = 0.234$

4) Nose shape

$x = 0.1 \qquad y = 0.078$

closely describes these blades (55). The equation

$$\pm y = 0.29690\sqrt{x} - 0.12600\,x - 0.35160\,x^2 + 0.28430\,x^3 - 0.10150\,x^4 \tag{2}$$

satisfies these conditions. Figure 1 shows a plot of this equation along with points obtained by removing the camber from the Göttingen 398 and Clark Y sections. Airfoils of any thickness can be obtained by applying the proper factor to equation 2,

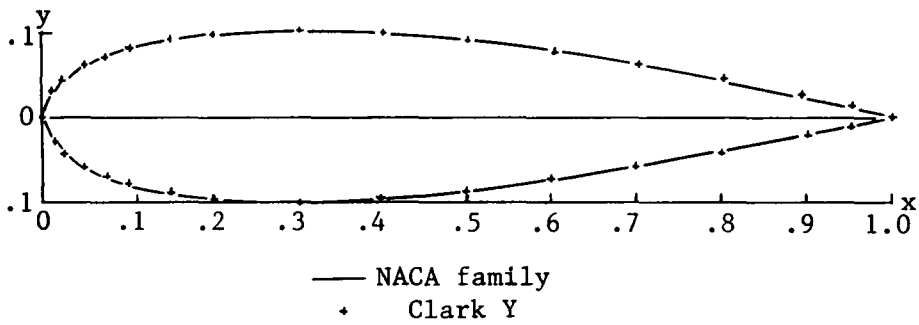

FIG. 1. BASIC ORDINATES OF NACA FAMILY AIRFOILS (as taken from reference 55)

$$\pm y_t = \frac{t}{0.20} (0.29690 \sqrt{x} - 0.12600\ x - 0.35160\ x^2 + 0.28430\ x^3 - 0.10150\ x^4) \tag{3}$$

where t is the maximum thickness of the desired airfoil.

The leading edge radius of airfoil sections defined by equation 1 is found to be

$$r_L = 1/2 \left(\frac{t}{0.20} A_o \right)^2 \tag{4}$$

Airfoils of different leading edge radius can be obtained by replacing the nose shape condition of equation 1 with the value of A_o obtained by solving equation 4 for the desired radius. Examples of the solution procedure are found in reference 54. Specification of a leading edge radius and a blade thickness, thus, completely defines the profile-thickness form.

A mean camber line can be defined by two parabolas of the form

$$y_c = B_0 + B_1\ x + B_2\ x^2 \tag{5}$$

Subject to the conditions (55),

1) Mean-line extremities

$x = 0$ $\qquad$ $y_c = 0$

$x = 1$ $\qquad$ $y_c = 0$

2) Maximum ordinate of mean line

$x = P$ (position of maximum ordinate)

$y_c = M$ (maximum ordinate)

$$\frac{dy_c}{dx} = 0$$

The resulting equations for the mean camber line are

$$y_c = \frac{M}{P^2} [2\ Px - x^2] \qquad 0 \leq x \leq P \tag{6}$$

and

$$y_c = \frac{M}{(1 - P)^2} [(1 - 2\ P) + 2\ Px - x^2] \qquad P \leq x \leq 1 \tag{7}$$

Differentiating these equations at the leading and trailing edge respectively,

$$\left.\frac{dy_c}{dx}\right|_0 = \frac{2M}{P} = \tan \gamma_1 \tag{8}$$

and

$$\left.\frac{dy_c}{dx}\right|_1 = \frac{2M}{P - 1} = \tan \gamma_2 \tag{9}$$

where γ_1 and γ_2 are the inlet and exit blade angles in the coordinate system of Figure 2. M and P can be determined in terms of γ_1 and γ_2.

$$P = \frac{1}{1 - \dfrac{\tan \gamma_1}{\tan \gamma_2}} \tag{10}$$

$$M = \frac{P}{2} \tan \gamma_1 \tag{11}$$

It is now possible to define the mean camber line by specifying γ_1 and

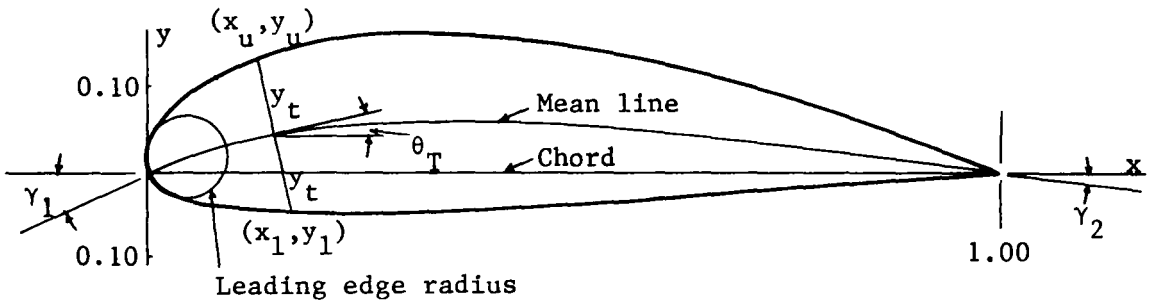

FIG. 2. DEVELOPMENT OF CAMBERED BLADE SECTION (as taken from reference 55)

γ_2 instead of M and P as done in reference 55.

The blade section is obtained by combining the profile-thickness form with the mean line form. Referring to figure 2, the ordinate y_t of the thickness form is measured perpendicular to the mean line from the point on the mean line corresponding to the value of x for which y_t was computed. The angle between the tangent to the mean line and the x axis is given by

$$\theta_T = \tan^{-1} \frac{dy_c}{dx} \tag{12}$$

The following formulas for calculating the blade profile coordinates may be derived,

$$x_u = x - y_t \sin \theta_T$$

$$y_u = y_c + y_t \cos \theta_T$$

$$x_l = x + y_t \sin \theta_T$$

$$y_l = y_c - y_t \cos \theta_T \tag{13}$$

where u and l refer to upper and lower surfaces respectively. Blade coordinates for chord lengths of other than 1.0 are found by multiplying the above coordinates by the desired chord length.

The blade shape thus obtained can be transformed into the coordinate system of a typical axial flow gas turbine. Referring to Figure 3,

$$\beta_1' = \gamma_1 - \alpha$$

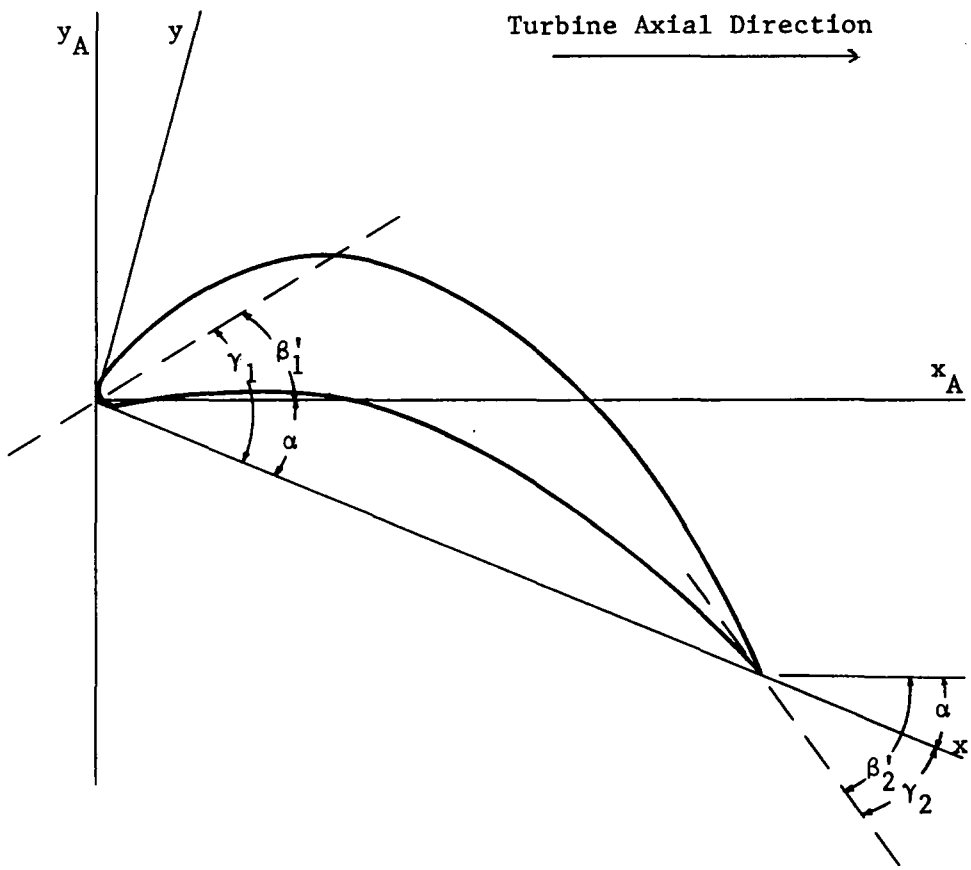

FIG. 3. BLADE SECTION - CHANGE OF COORDINATE AXES

$$\beta_2' = \gamma_2 + \alpha \tag{14}$$

where β_1' and β_2' are the inlet and exit blade angles respectively in the gas turbine coordinate system and α is the stagger angle. The blade profile coordinates are transformed by

$$x_A = x \cos \alpha + y \sin \alpha$$

$$y_A = x \sin \alpha - y \cos \alpha \tag{15}$$

where A refers to the gas turbine reference frame.

Using the method described above, it is possible to generate a turbine blade form by specifying the inlet angle, exit angle, maximum thickness, chord length, stagger angle, and leading edge radius.

Two-Dimensional Inviscid Main Flow

(Following the Development of Reference 1)

A fortran program for calculating transonic velocities on a blade-to-blade stream surface of a turbomachine was developed by Katsanis (50). The following assumptions were made in the development of that program:

"1. The flow is steady relative to the blade.

2. The fluid is a perfect gas with zero viscosity.

3. The flow is isentropic and free of vortices.

4. The velocity component normal to the blade-to-blade surface is zero.

5. The stagnation temperature is uniform across the inlet.
6. The velocity magnitude and direction are uniform across both the upstream and downstream boundaries.
7. The flow is essentially subsonic with only locally supersonic spots."

The calculations are performed on a blade-to-blade surface of revolution as shown in Figure 4. The meridional streamline distance, m, and θ are the independent variables. The solution is obtained by reducing the weight flow until the entire flow is subsonic. The subsonic case is solved and the velocity distribution for the full flow determined using velocity gradient techniques.

For the reduced weight flow, the stream function, ψ, is defined by

$$\frac{\partial\psi}{\partial\theta} = \frac{rh\rho}{W} W_m$$

$$\frac{\partial\psi}{\partial m} = -\frac{h\rho}{W} W_\theta \tag{16}$$

and is governed by

$$\frac{\partial^2\psi}{\partial m^2} + \frac{1}{r^2}\frac{\partial^2\psi}{\partial\theta^2} - \frac{1}{r^2\rho}\frac{\partial\rho}{\partial\theta}\frac{\partial\psi}{\partial\theta} + \left[\frac{\sin\lambda}{r} - \frac{1}{\rho h}\frac{\partial(\rho h)}{\partial m}\right]$$

$$\frac{\partial\psi}{\partial m} = \frac{2h\rho}{W}\omega\sin\lambda \tag{17}$$

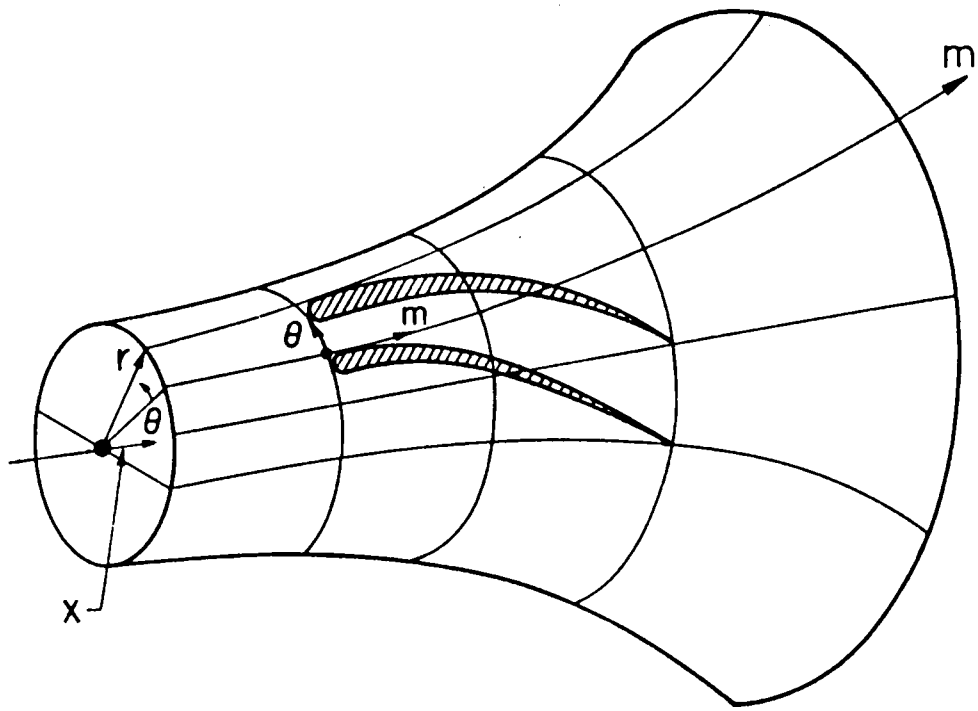

FIG. 4. BLADE - TO - BLADE STREAM SURFACE OF REVOLUTION (as taken from reference 1)

The temperature distribution is obtained from the energy equation,

$$\frac{T}{T_i} = 1 - \frac{(W_m{}^2 + W_\theta{}^2) + 2\ \omega\ \varepsilon_i - (\omega r)^2}{2\ C_p\ T_i} \tag{18}$$

The density distribution is determined from the isentropic relation,

$$\frac{\rho}{\rho_i} = \left(\frac{T}{T_i}\right)^{\frac{k}{k-1}} \tag{19}$$

Boundary conditions are summarized in Figure 5. The equation governing ψ is elliptic and is solved using a finite difference technique.

When the flow is locally supersonic equation 17 is no longer elliptic throughout the region. A different solution technique is, therefore, necessary. The method used is based on the velocity gradient equation

$$\frac{\partial W}{\partial \theta} = AW + B \tag{20}$$

where

$$A = r^2 \cos^2\beta\ \frac{d^2\theta}{dm^2} + \sin\lambda\ \tan\beta\ (1 + \cos^2\beta) \tag{21A}$$

on the blade surface,

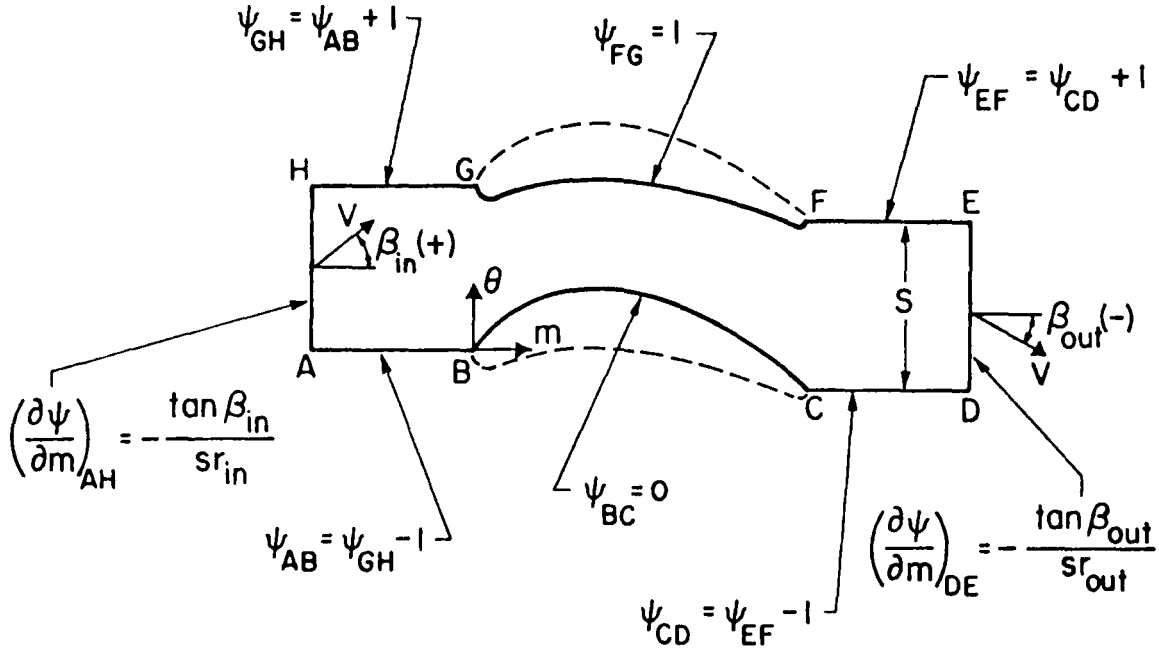

FIG. 5. STREAM CHANNEL BOUNDARY CONDITIONS (as taken from reference 1)

$$A = \sin^2\beta \left[2 \frac{\frac{\partial^2\psi}{\partial\theta\,\partial m}}{\frac{\partial\psi}{\partial m}} - \frac{\frac{\partial\psi}{\partial\theta}}{\left(\frac{\partial\psi}{\partial m}\right)^2} \frac{\partial^2\psi}{\partial m^2} - \frac{\frac{\partial^2\psi}{\partial\theta^2}}{\frac{\partial\psi}{\partial\theta}} \right] +$$

$$\sin\lambda \tan\beta \,(1 + \cos^2\beta) \tag{21B}$$

at interior points, and

$$B = r \tan\beta \frac{\partial W}{\partial m} + \frac{2\,\omega r \sin\lambda}{\cos\beta} \tag{22}$$

The full weight flow velocity distribution is calculated by solving equation 20 in conjunction with the continuity equation,

$$\int_{\theta_1}^{\theta_2} \rho\, W \cos\beta\, hr\, d\theta = W \tag{23}$$

The Katsanis main flow solution does not include boundary layers on the blade, hub, or casing. Whether these effects significantly alter turbine blade erosion is not known.

Particle Trajectory and Erosion Model

(Following the Development of Reference 1)

Turbine blade erosion is conventionally determined in two steps. First, the particle trajectories in the turbine blade passage are determined; then, the erosion corresponding to each particle impact is obtained. The particle trajectory program of Menguturk and

Sverdrup (1) takes this approach. The development of that program is summarized below.

The only significant forces acting on a small solid particle in a low density-high velocity fluid flow are the viscous drag force and inertia of the particle. For a spherical particle the drag force is given by

$$\vec{F}_D = 3\pi \mu_G d_p (\vec{V}_G - \vec{V}_p) f(R_e) \tag{24}$$

where

$$f(R_e) = C_D \frac{R_e}{24}$$

The drag coefficients at different Reynolds numbers are:

$$\begin{aligned}
C_D &= 24/R_e && (0 < R_e \leq 0.1) \\
C_D &= 22.73/R_e + 0.093/(R_e)^2 + 3.69 && (0.1 < R_e \leq 1) \\
C_D &= 38.80/R_e - 12.65/(R_e)^2 + 0.36 && (1 < R_e \leq 10) \\
C_D &= 46.50/R_e - 116.661/(R_e)^2 + 0.61667 && (10 < R_e \leq 100) \\
C_D &= 98.33/R_e - 2778/(R_e)^2 + 0.3644 && (100 < R_e \leq 1000) \\
C_D &= 148.62/R_e - 47500/(R_e)^2 + 0.35714 && (1000 < R_e \leq 5000)
\end{aligned} \tag{25}$$

where

$$R_e = \frac{\rho_g d_p \mid V_G - V_p \mid}{\mu_g} \tag{26}$$

The equations of motion of the particle are determined by equating the particle inertia to the drag force. In x, r, θ coordinates the equations of motion are:

$$\ddot{x}_p = G(V_x - \dot{x}_p)$$

$$\ddot{\theta}_p = \frac{G}{r}(V_\theta - r\dot{\theta}) - \frac{2\dot{r}_p}{r}(\dot{\theta}_p + \omega)$$

$$\ddot{r}_p = G(V_r - \dot{r}_p) + r(\dot{\theta}_p + \omega)^2 \tag{27}$$

where

$$G = \frac{18\,\mu_g}{d_p^{\,2}\,\rho_p} f\,(R_e) \tag{28}$$

The particle's path is determined by numerically integrating equation 27 until collision with the blade surface. The path of the particle after collision is determined from the rebound data of Hussein (44). This experimental data, shown in Figure 6, can be approximated by the equations:

$$\frac{V_{p_2}}{V_{p_1}} = \frac{V_{p_{n2}}}{V_{p_{n1}}} \left[\frac{1 + \cot^2\beta_2}{1 + \cot^2\beta_1}\right]^{\frac{1}{2}}$$

$$\frac{\beta_2}{\beta_1} = \frac{1}{\beta_1}\cot^{-1}\left[\frac{V_{p_{t2}}}{V_{p_{t1}}}\,\frac{V_{p_{n1}}}{V_{p_{n2}}}\right]\cot\beta_1$$

$$\frac{V_{p_{t2}}}{V_{p_{t1}}} = 0.95 + 0.00055\,\beta_1$$

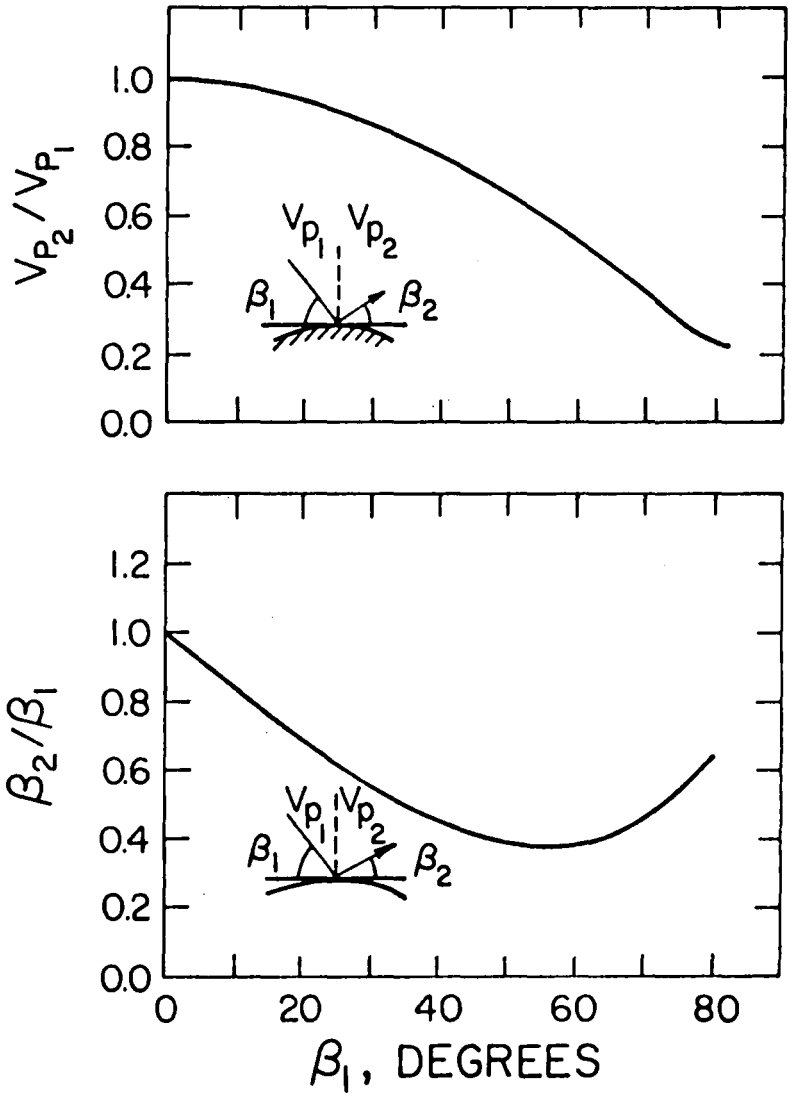

FIG. 6. PARTICLE REBOUND DATA (as taken from reference 1)

$$\frac{V_{p_{n2}}}{V_{p_{n1}}} = 1.0 - 0.02108\ \beta_1 + 0.0001417\ \beta_1^2 \tag{29}$$

Having obtained the particle trajectories, the erosion corresponding to each particle impact may be expressed by the following equation according to Bitter (33, 34),

$$S = \frac{1}{2} M_1 \frac{(V_p^{\ 2} \cos^2 \beta_1 - V_{p_{tr}}^{\ 2})}{\phi} + \frac{1}{2} M_1 \frac{(V_p \sin \beta_1 - V_{p_{eL}})^2}{\varepsilon} \tag{30}$$

where S is the volume of material lost due to erosion and M_1 is the mass of the impinging particles. The first term of Equation 30 represents the ductile mode of erosion; the second term represents the brittle mode of erosion.

Equation 30 can be rewritten as

$$E = \frac{S}{M_1} = K_1 (V_p \cos \beta_1)^{m_1} \left[1 - \left(\frac{V_{p_{tr}}}{V_p \cos \beta_1} \right)^{m_1} \right] + K_2 \ (V_p \sin \beta_1 - V_{p_{eL}})^{m_2} \tag{31}$$

introducing the generalized velocity exponents m_1 and m_2 and the coefficients K_1 and K_2 to define the amplitude of the ductile and brittle modes respectively. The term in brackets can be made a

function of the impact angle, β_1, only. Equation 31 can then be rewritten

$$E = K_1 (V_p \cos \beta_1)^{m_1} f(\beta_1) + K_2 (V_p \sin \beta_1 - V_{p_{eL}})^{m_2} \tag{32}$$

where

$$f(\beta_1) = \begin{cases} \sin (n \beta_1) & \text{for } \beta_1 \leq \beta_0 \\ 1 & \text{for } \beta_1 > \beta_0 \end{cases}$$

is chosen so that the erosion rate as a function of impact angle fits experimental results. Neglecting $V_{p_{eL}}$ and assuming $m_1 = m_2 = m_0$ the erosion equations become:

$$\begin{aligned} E &= K_1(V_p \cos \beta_1)^{m_0} \sin (n \beta_1) + K_2 (V_p \sin \beta_1)^{m_0} \quad \text{for } \beta_1 \leq \beta_0 \\ E &= K_1(V_p \cos \beta_1)^{m_0} + K_2 (V_p \sin \beta_1)^{m_0} \quad \text{for } \beta_1 > \beta_0 \end{aligned} \tag{33}$$

Typical results of these equations are shown in Figure 7. The coefficients K_1, K_2, m_0, and β_0 must be determined experimentally. For silicon carbide particles striking nickel cobalt alloy, m_0 is assumed to be 2.5 and the following experimental results by Smeltzer (56) may be used:

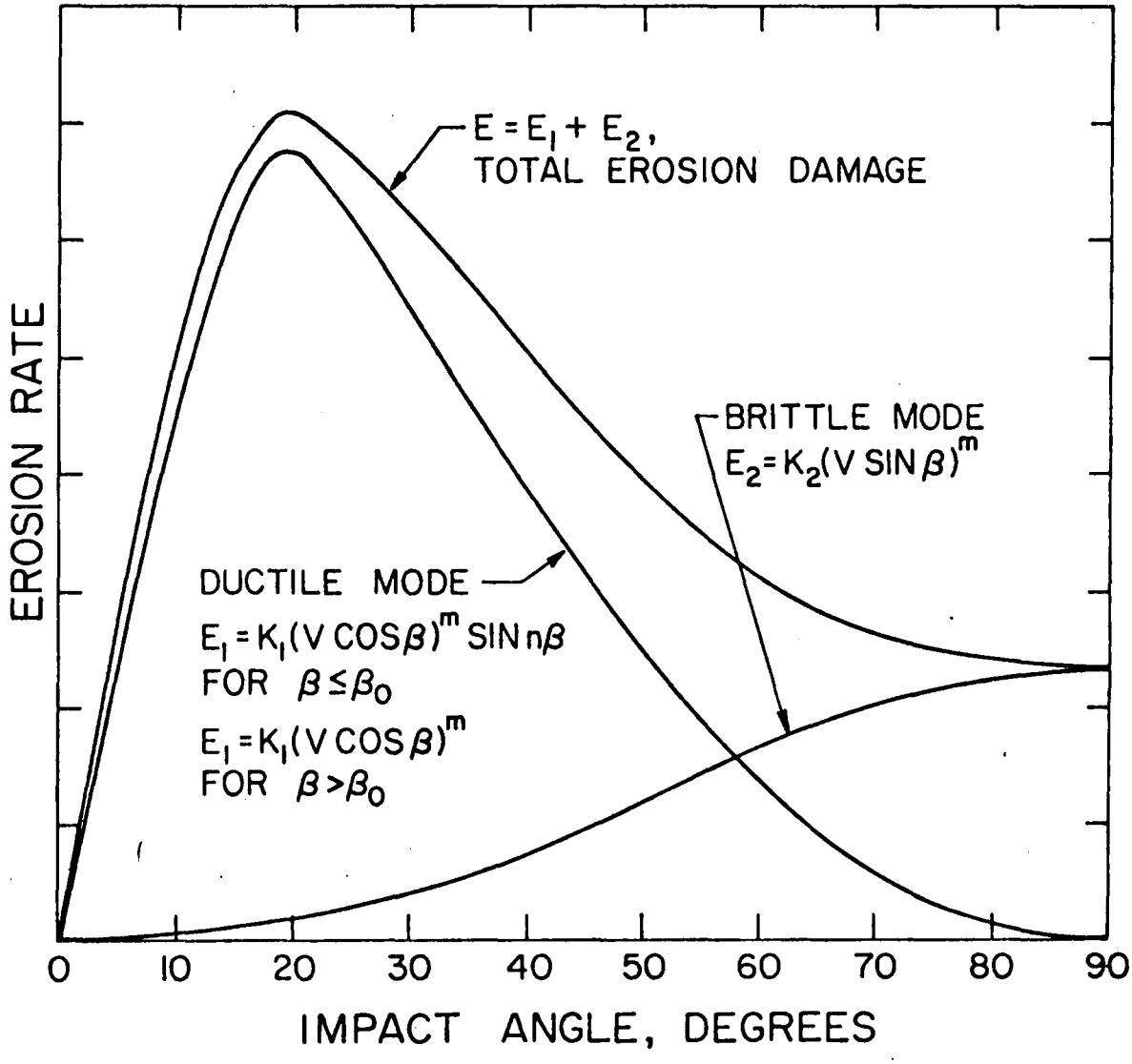

FIG. 7. BRITTLE AND DUCTILE MODES OF EROSION (as taken from reference 1)

β_{max} (deg.)	β_0 (deg.)	$K_1 \frac{mm^3/Gm}{(ft/sec)^2}$	$K_2 \frac{mm^3/Gm}{(ft/sec)^2}$
10	10.3	7.44×10^{-8}	2.4×10^{-8}
20	22.7	8.35×10^{-8}	2.4×10^{-8}
30	45.3	1.12×10^{-7}	2.4×10^{-8}
90	90	0	7.18×10^{-8}

Comparison of erosion by silicon carbide particles with erosion by coal ash particles (26), indicates silicon carbide particles to be 25 times as erosive as coal ash particles. In this way, the data of Smeltzer may be extended to erosion by coal ash particles.

Degree of Reaction

Degree of reaction is defined by

$$\Lambda = \frac{T_2 - T_3}{T_1 - T_3} \tag{34}$$

for an axial flow turbine. Part of this investigation required a method of varying degree of reaction while maintaining constant work across the turbine stage.

With reference to Figure 8, a relationship for Λ can be determined in terms of the flow angles and velocities in the turbine passage.

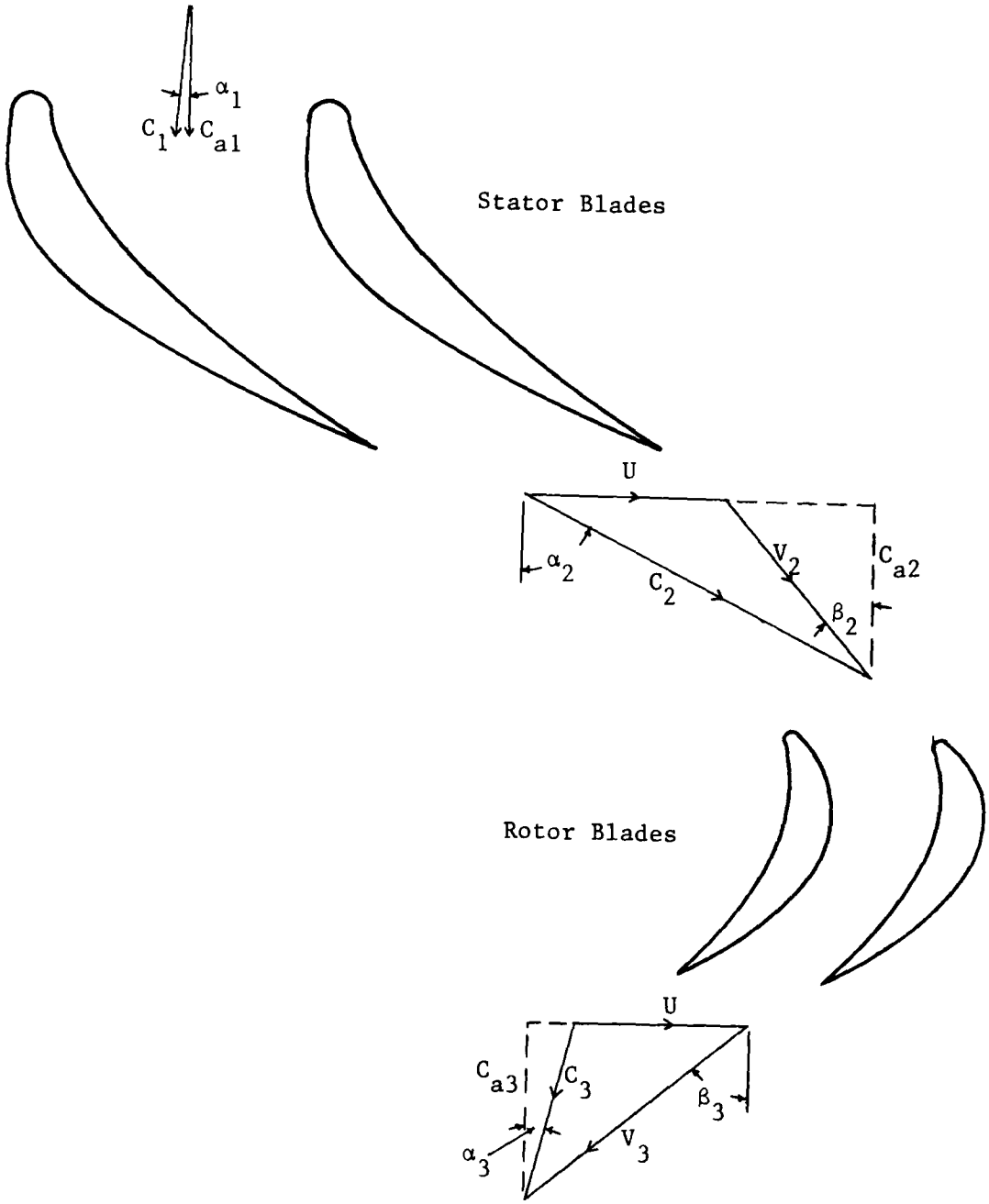

FIG. 8. VELOCITY TRIANGLES FOR AN AXIAL FLOW TURBINE STAGE

For $C_a \neq$ constant and $C_1 \neq C_3$ the relationship is derived as follows.

The stage work is given by

$$W_s = C_p (T_{01} - T_{03})$$

$$= C_p (T_1 - T_3) + 1/2 (C_1^2 - C_3^2)$$

$$= U (V_2 \sin \beta_2 + V_3 \sin \beta_3) \tag{35}$$

Then,

$$\Delta h_{static} = C_p (T_1 - T_3)$$

$$= U(V_2 \sin \beta_2 + V_3 \sin \beta_3) + 1/2 (C_3^2 - C_1^2) \tag{36}$$

Relative to the rotor blades the flow does no work and the energy equation yields

$$C_p (T_2 - T_3) = 1/2 (V_3^2 - V_2^2) \tag{37}$$

The relationship for Λ is, therefore,

$$\Lambda = \frac{1/2 (V_3^2 - V_2^2)}{\Delta h_{static}}$$

$$= \frac{1/2 (V_3^2 - V_2^2)}{U(V_2 \sin \beta_2 + V_3 \sin \beta_3) + 1/2 (C_3^2 - C_1^2)} \tag{38}$$

One approach to varying Λ is to keep W_s and Δh_{static} constant when Λ is changed. From the definitions of W_s and Δh_{static}, C_3 also

remains constant. C_2 can be determined directly since,

$$\Delta h_{static} = C_p\ (T_1 - T_2) + C_p\ (T_2 - T_3)$$

$$= 1/2\ (C_2^2 - C_1^2) + 1/2\ (V_3^2 - V_2^2) \tag{39}$$

and

$$\Lambda = \frac{1/2\ (V_3^2 - V_2^2)}{\Delta h_{static}}$$

$$= \frac{\Delta h_{static} - 1/2\ (C_2^2 - C_1^2)}{\Delta h_{static}} \tag{40}$$

The remaining unknowns V_2, V_3, β_2, β_3, α_2, and α_3 are determined by simultaneously solving the equations for W_s and Λ with 4 equations relating the flow angles and velocities. These equations are:

$$V_2 \cos \beta_2 = C_2 \cos \alpha_2$$

$$V_3 \cos \beta_3 = C_3 \cos \alpha_3$$

$$U = C_2 \sin \alpha_2 - V_2 \sin \beta_2$$

$$U = V_3 \sin \beta_3 - C_3 \sin \alpha_3 \tag{41}$$

X. PARAMETER VARIATIONS

The purpose of this investigation is to determine the effect of blade profile variations on the erosion of gas turbine blades. Variations of the blade exit angle and leading edge radius were studied as well as one variation of degree of reaction.

The mean blade profiles were chosen to be the first stage stator and rotor of the Westinghouse Model 501 B axial flow turbine. Blade profiles were obtained using the blade model previously described (55) which closely resemble the Westinghouse blades. This was accomplished by minimizing the variance between the blade model profile and 18 discrete profile points of both the Westinghouse stator and rotor. The resulting blade sections are shown in Figure 9. Having made an approximation of the Model 501 B first stage, any desired profile changes could be obtained by making the appropriate changes in the blade model input.

As seen in Figure 9, the exit angles of the stator and rotor are 68.7° and 58.1° respectively. The blade exit angle profile variation was accomplished by producing stator and rotor blade sections using the blade model with exit angles reduced by 2.5°, 5.0°, and 7.5°. These blades are compared with the Westinghouse stator and rotor in Figures 10 and 11, respectively.

The leading edge radius variation was handled similarly. Blade profiles were produced using the blade model with leading edge radii of $1/2\ R_1$ and $1.67\ R_1$ for the stator and $1/4\ R_2$ and $3\ R_2$ for the rotor. R_1 is the leading edge radius of the Westinghouse stator.

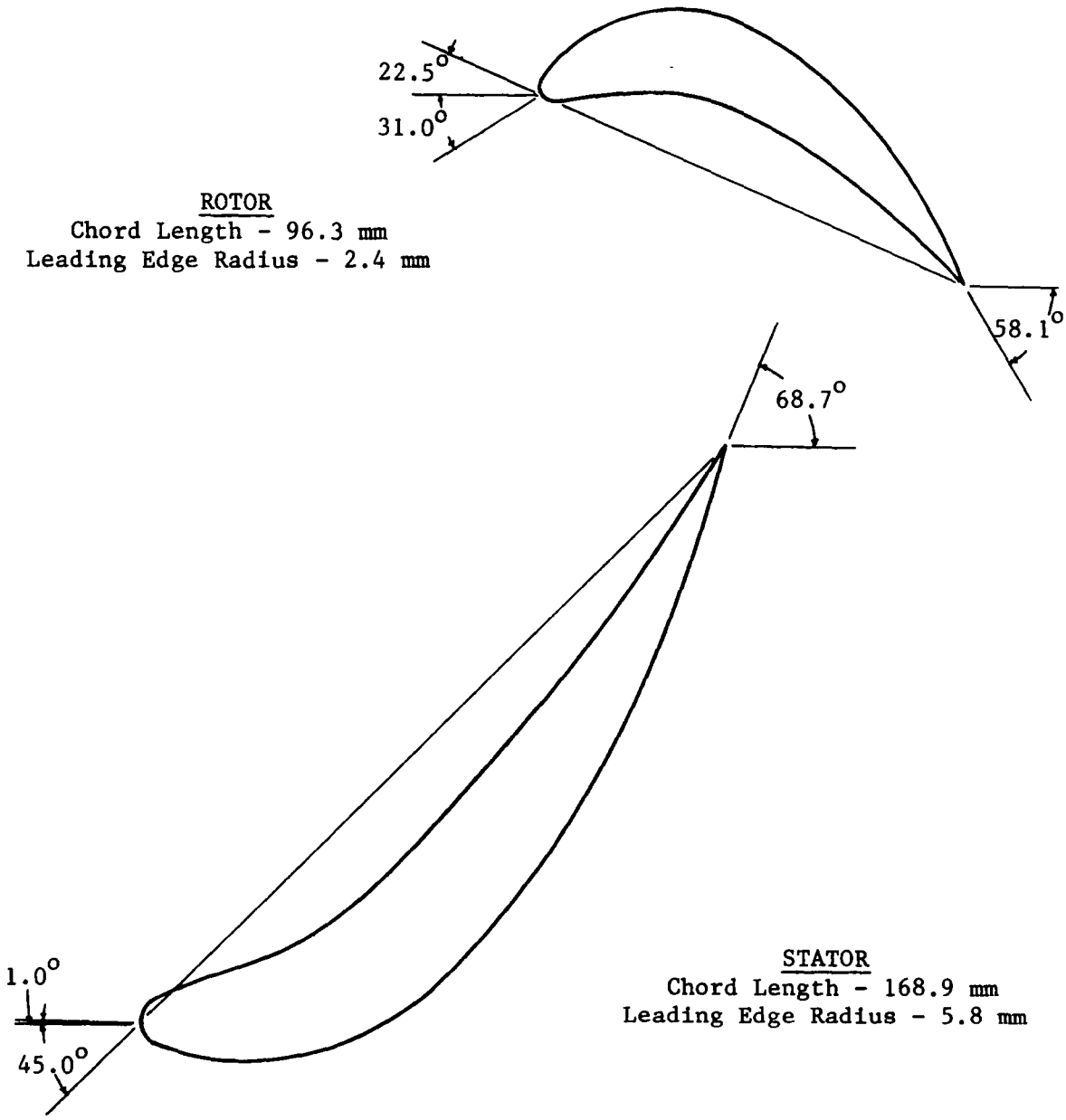

FIG. 9. BLADE MODEL APPROXIMATION OF THE WESTINGHOUSE MODEL 501B FIRST STAGE

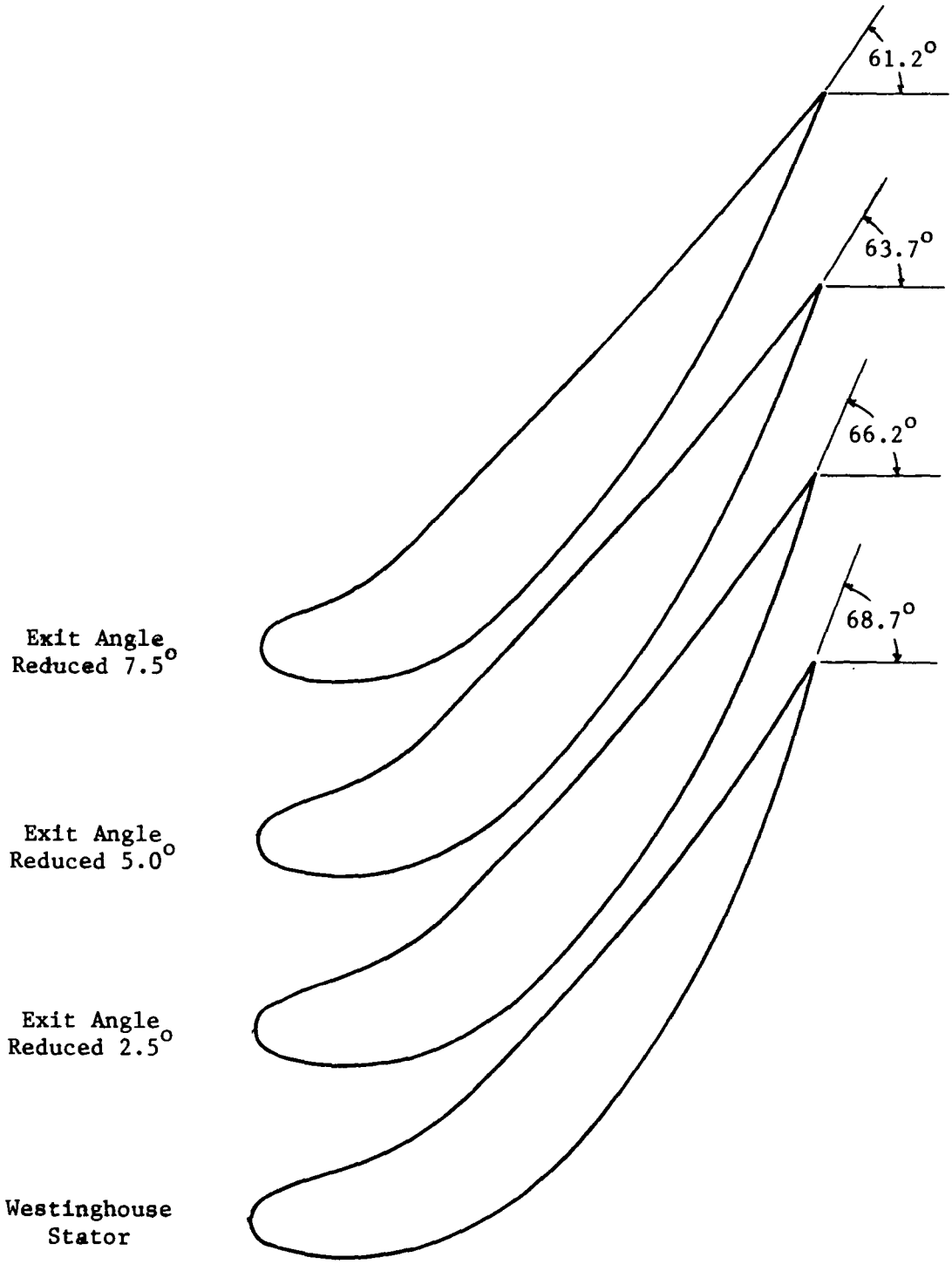

Fig. 10. BLADE EXIT ANGLE VARIATION FOR STATOR

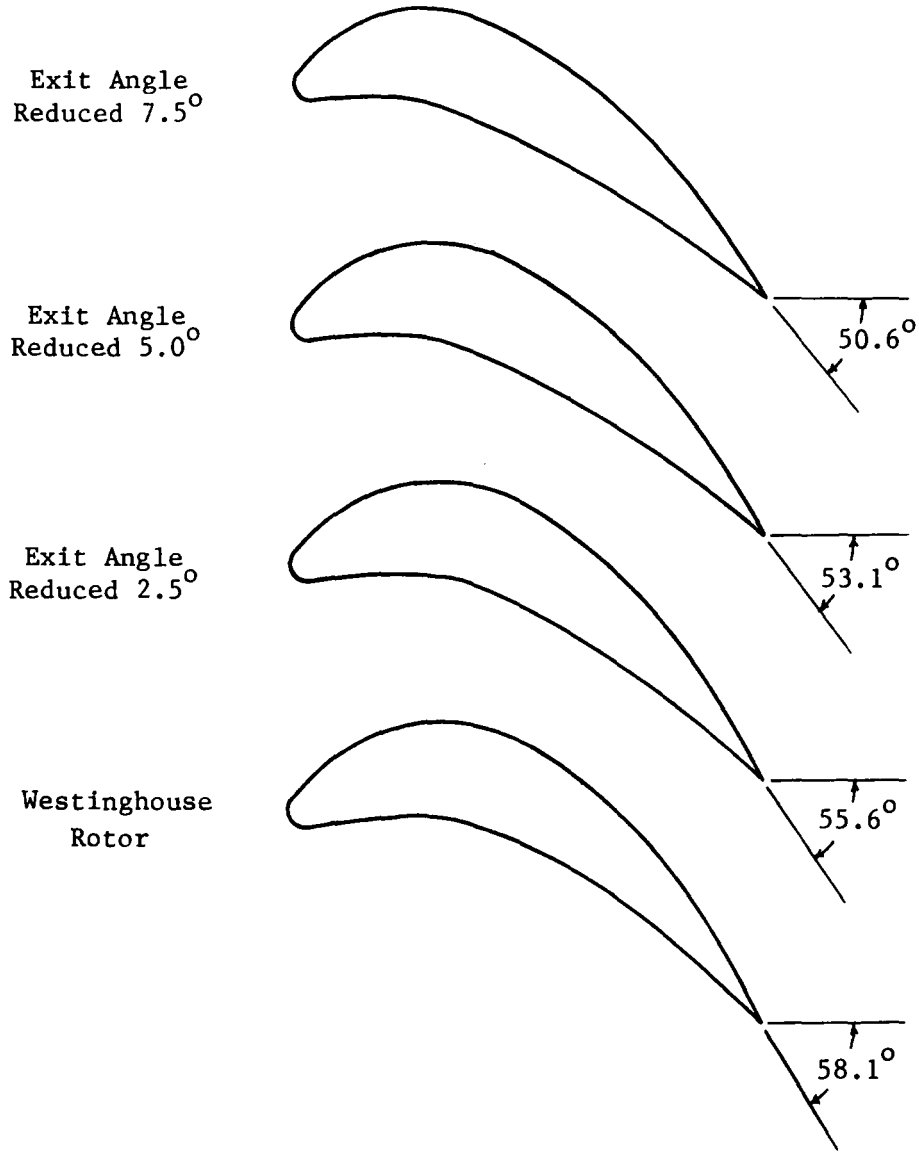

FIG. 11. BLADE EXIT ANGLE VARIATION FOR ROTOR

R_2 is the leading edge radius of the Westinghouse rotor. These blades are plotted along with the Westinghouse stator and rotor in Figures 12 and 13 respectively.

The flow field of the blade passage bounded by each of the above blades was determined using the Katsanis computer program. The weight flow used was 10 percent less than that of the Westinghouse Model 501B turbine to avoid choking in the blade passages. Thus, the velocities in the blade passages were lower than those of the Westinghouse turbine though the relative gas angles were kept constant. Due to the elliptic nature of the Katsanis flow model, a certain amount of iteration was necessary to obtain the correct flow exit angle.

The flow field of each turbine passage was then entered into the erosion model as well as the initial conditions of 19 particles. More accurate results could have been obtained by increasing the number of particles in the blade passage, however, 19 was the maximum allowed by the erosion program.

The initial particle conditions for the stator and rotor are shown in Tables 1 and 2 respectively. The initial particle conditions for the rotor were determined from the particle trajectories at the stator exit.

A particle size of 10μm was used because, though separation equipment will keep their concentration low, 10μm particles will still cause the greatest erosion (19, 26). A particle density of 1.5 gm/cc was used. This corresponds to the density of typical coal ash

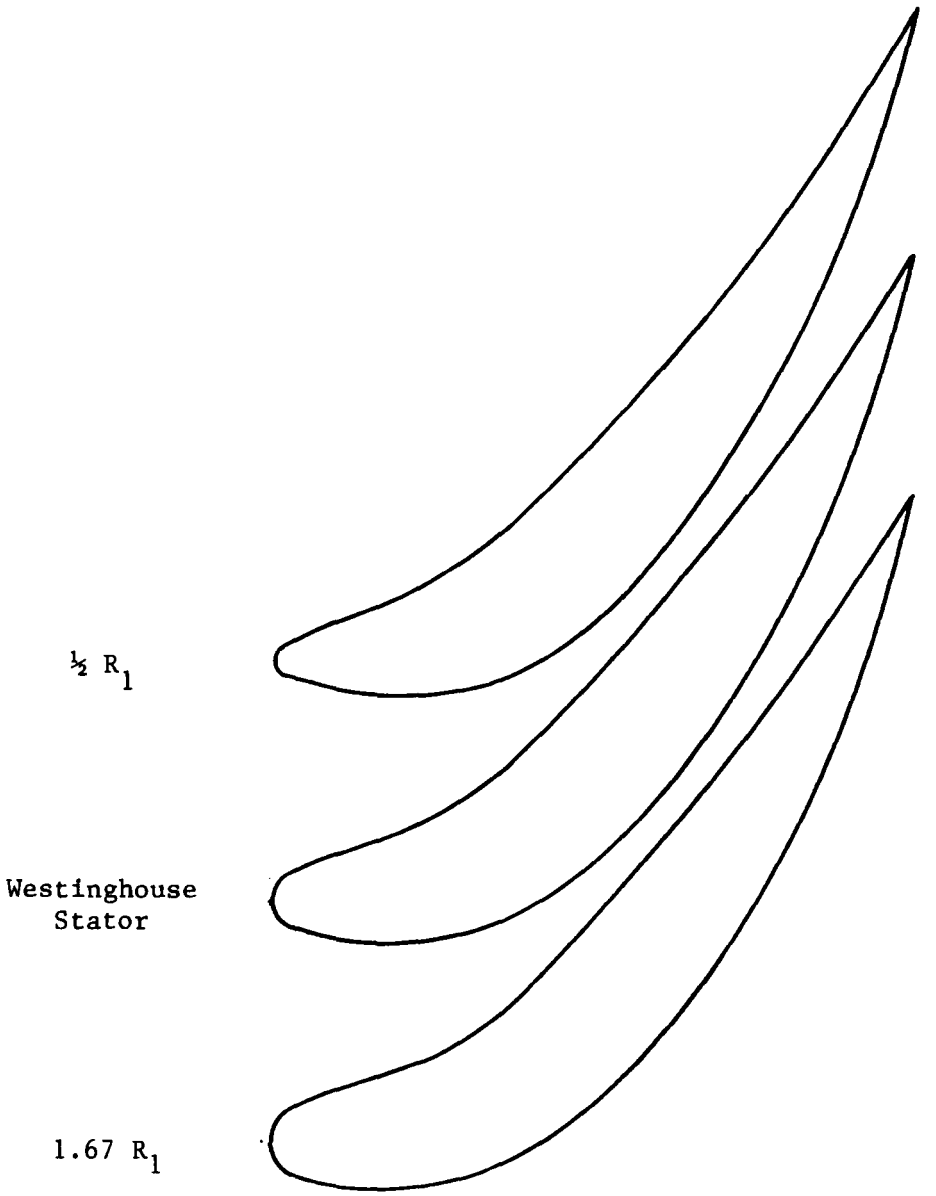

FIG. 12. LEADING EDGE RADIUS VARIATION FOR STATOR

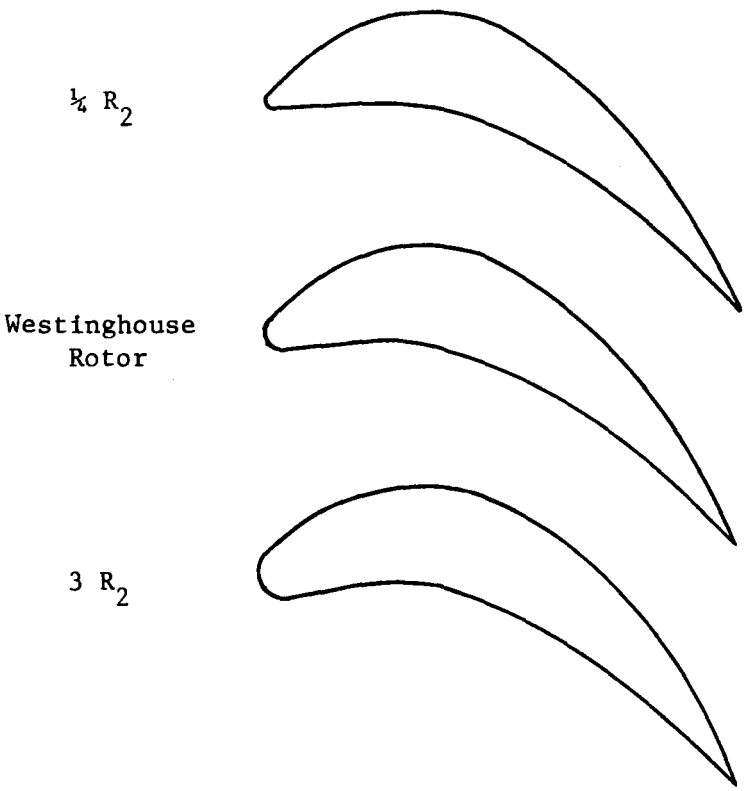

FIG. 13. LEADING EDGE RADIUS VARIATION FOR ROTOR

TABLE 1. INITIAL PARTICLE CONDITIONS FOR STATOR BLADES

d_p = 10μm α_p = 0°

ρ_p = 1.5 gm/cc β_p = 0°

V_p = 168 m/s x = -0.046 m

Particle Number	θ (Radians)
1	0.00
2	0.006889
3	0.013778
4	0.020668
5	0.027558
6	0.034447
7	0.041337
8	0.048226
9	0.055115
10	0.062005
11	0.068895
12	0.075784
13	0.082674
14	0.089563
15	0.096453
16	0.103342
17	0.110230
18	0.117121
19	0.124010

TABLE 2. INITIAL PARTICLE CONDITIONS FOR EXIT ANGLE AND LEADING EDGE RADIUS VARIATION OF ROTOR

d_p = 10μm α_p = 1.52°

ρ_p = 1.5 gm/cc β_p = 23.9°

V_p = 295 m/s x = -0.005 m

Particle Number	θ (Radians)
1	0.00
2	0.003481
3	0.006962
4	0.010443
5	0.013924
6	0.017405
7	0.020886
8	0.024367
9	0.027848
10	0.031323
11	0.034809
12	0.038291
13	0.041772
14	0.045252
15	0.048734
16	0.052215
17	0.055696
18	0.059177
19	0.062658

particles.

The degree of reaction of the model 501B turbine is 0.167. One variation of this degree of reaction was investigated, that being a degree of reaction of zero.

The procedure for changing degree of reaction is described in the analysis section. The following flow angles and velocities were obtained for $\Lambda = 0$:

$\beta_2 = 52.5^o$ $\beta_3 = 48.5^o$

$\alpha_2 = 67.9^o$ $\alpha_3 = 4.4^o$

$C_2 = 715$ m/s $C_3 = 293$ m/s

$V_2 = V_3 = 441$ m/s

Blade sections were generated with the blade model until a stator and rotor were obtained which satsify the above flow angles and velocities. The stator and rotor corresponding to $\Lambda = 0$ are compared with the model 501B first stage in Figure 14.

The erosion of the zero degree of reaction stage was determined as described previously except that the initial particle conditions for the rotor were changed. This is because the stator exit angle is increased when Λ is reduced, and thus, the particle trajectories at the stator exit are changed. The initial particle conditions for the $\Lambda = 0$ rotor are shown in Table 3.

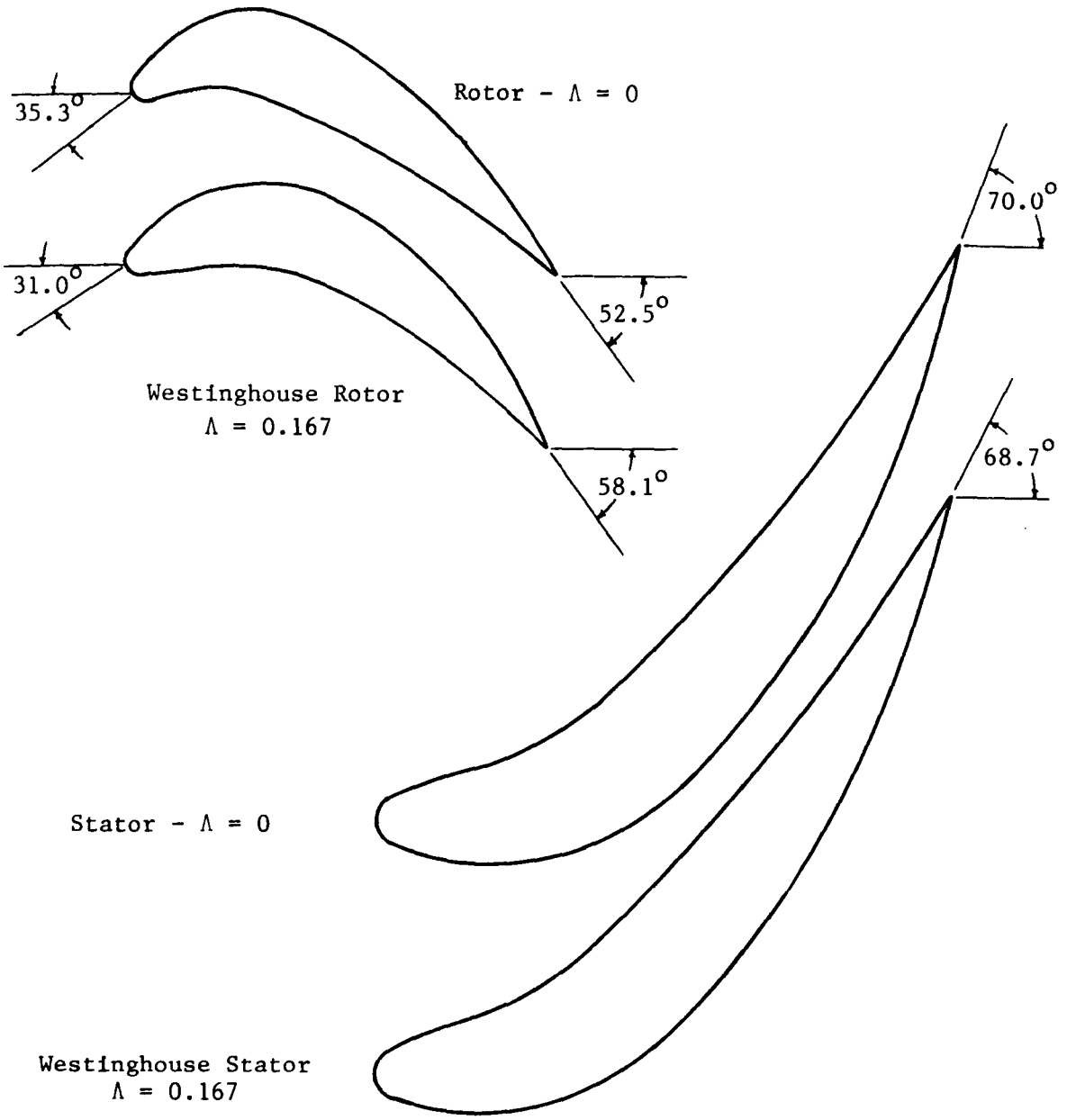

FIG. 14. COMPARISON OF THE WESTINGHOUSE MODEL 501B FIRST STAGE WITH A ZERO DEGREE OF REACTION STAGE

TABLE 3. INITIAL PARTICLE CONDITIONS FOR ROTOR OF ZERO DEGREE OF REACTION STAGE

d_p = 10μm α_p = 1.52°

ρ_p = 1.5 gm/cc β_p = 24.9°

V_p = 320 m/s x = -0.005

Particle Number	θ (Radians)
1	0.00
2	0.003481
3	0.006962
4	0.010443
5	0.013924
6	0.017405
7	0.020886
8	0.024367
9	0.027848
10	0.031323
11	0.034809
12	0.038291
13	0.041772
14	0.045252
15	0.048734
16	0.052215
17	0.055696
18	0.059177
19	0.062658

XI. RESULTS AND DISCUSSION

The erosion of the Westinghouse Model 501B first stage stator and rotor as a function of axial distance from the blade leading edge is shown in Figures 15 and 16, respectively. The results are presented for both SiC particles and coal ash particles. The damage caused by SiC particles is presented in terms of the volume, mm^3, removed per millimeter of blade surface length per kilogram of particles entering the blade passage. The results are modified for coal ash particles and expressed as millimeters of metal recession in 10,000 hours assuming an inlet particle concentration of 2×10^{-7} kg/kg of expansion gas. Details of the procedure for obtaining metal recession due to coal ash particles from the erosion rate of SiC particles is shown in Appendix A. Only the erosion of the blade pressure surfaces is plotted since the particle impacts on the suction surfaces are confined to the leading edge.

As seen in Figure 15, the erosion of the stator remains low over most of the blade surface but sharply increases near the trailing edge. This is due to the high impact velocities and frequency of impact near the trailing edge.

The erosion of the rotor has slightly different characteristics. As seen in Figure 16, there is considerable damage to the rotor leading edge. This is followed by a region of low erosion with a sharp increase in erosion near the trailing edge.

In both of these figures, sharp changes occur in the erosion

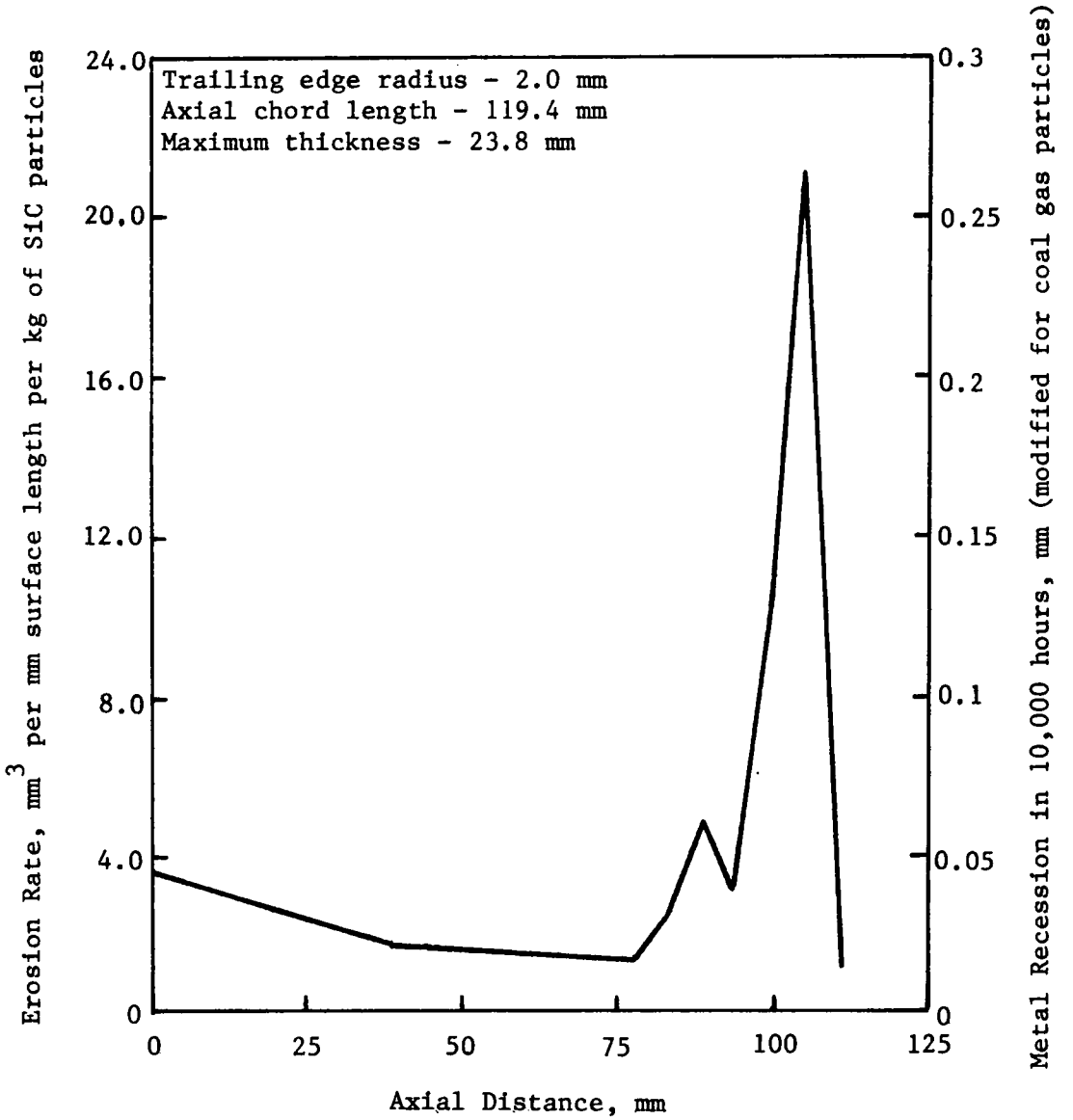

FIG. 15. EROSION RATE IN WESTINGHOUSE STATOR AS A FUNCTION OF AXIAL POSITION

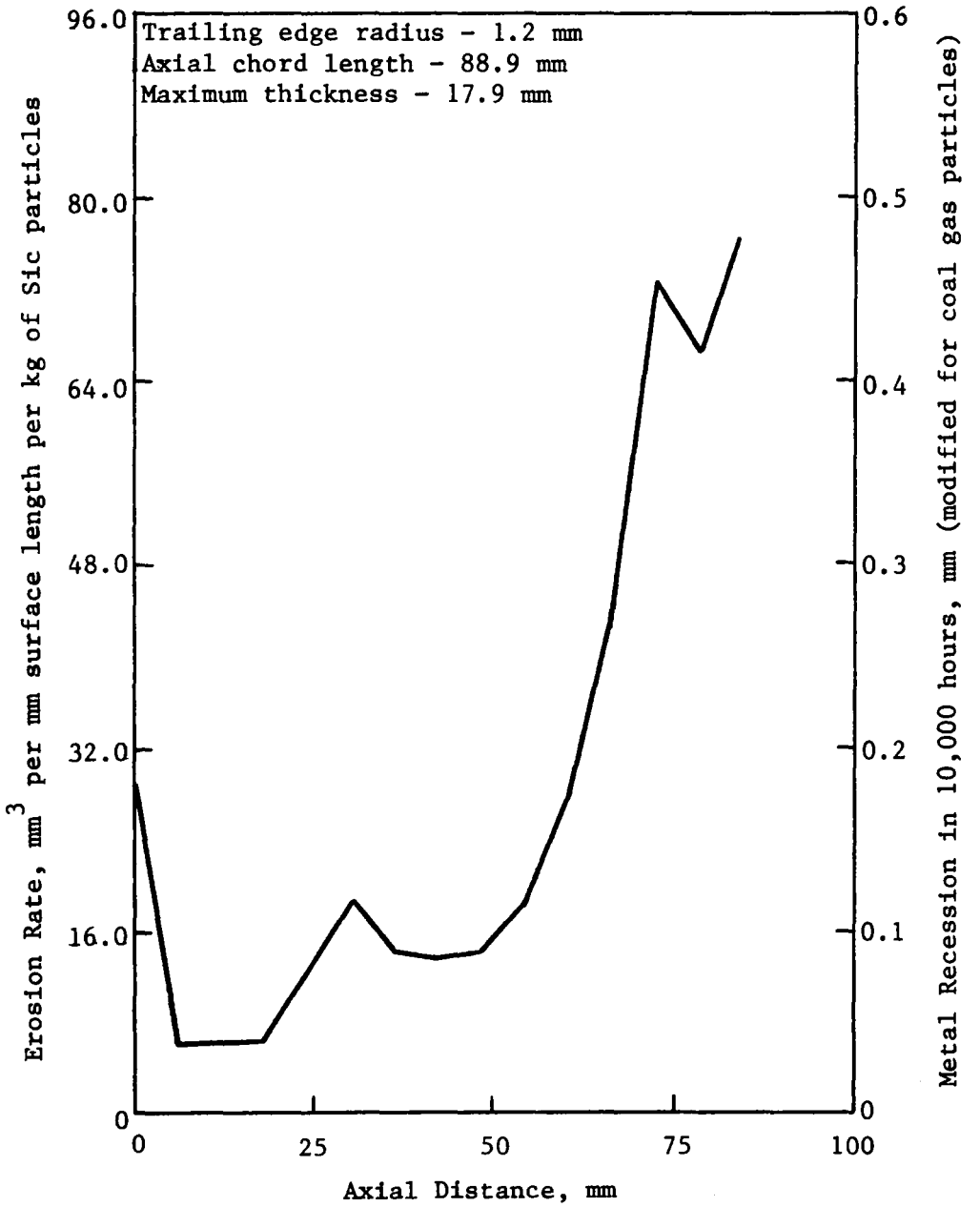

FIG. 16. EROSION RATE IN WESTINGHOUSE ROTOR AS A FUNCTION OF AXIAL POSITION

rate along the blade surface. These changes are physically unreasonable and are due to the discrete nature of the erosion calculations.

From these figures, it can be seen that the erosion of the trailing edge of the stator and rotor and the erosion of the leading edge of the rotor are of critical importance in the design of coal-fired turbine blades. The results of the blade profile variations are, therefore, presented in terms of the erosion at these blade stations. To this end, leading and trailing edge erosion were defined as the average erosion over the first and last 20 percent of the blade, respectively. This approach was necessary in order to smooth the variations in erosion in each finite difference interval along the blade surface.

The erosion of each blade profile investigated as a function of axial distance from the leading edge is shown in Appendix B. The corresponding particle trajectory plots are shown in Appendix C.

Stator

The trailing edge erosion of the stator as a function of reduction in the blade exit angle is shown in Figure 17. As can be seen in the figure, the trailing edge erosion increases as the blade angle is increased. This is due to the increased impact velocities and frequency of impact at higher blade angles. The scatter of the erosion data points is due to the small number of particles input into the blade passage.

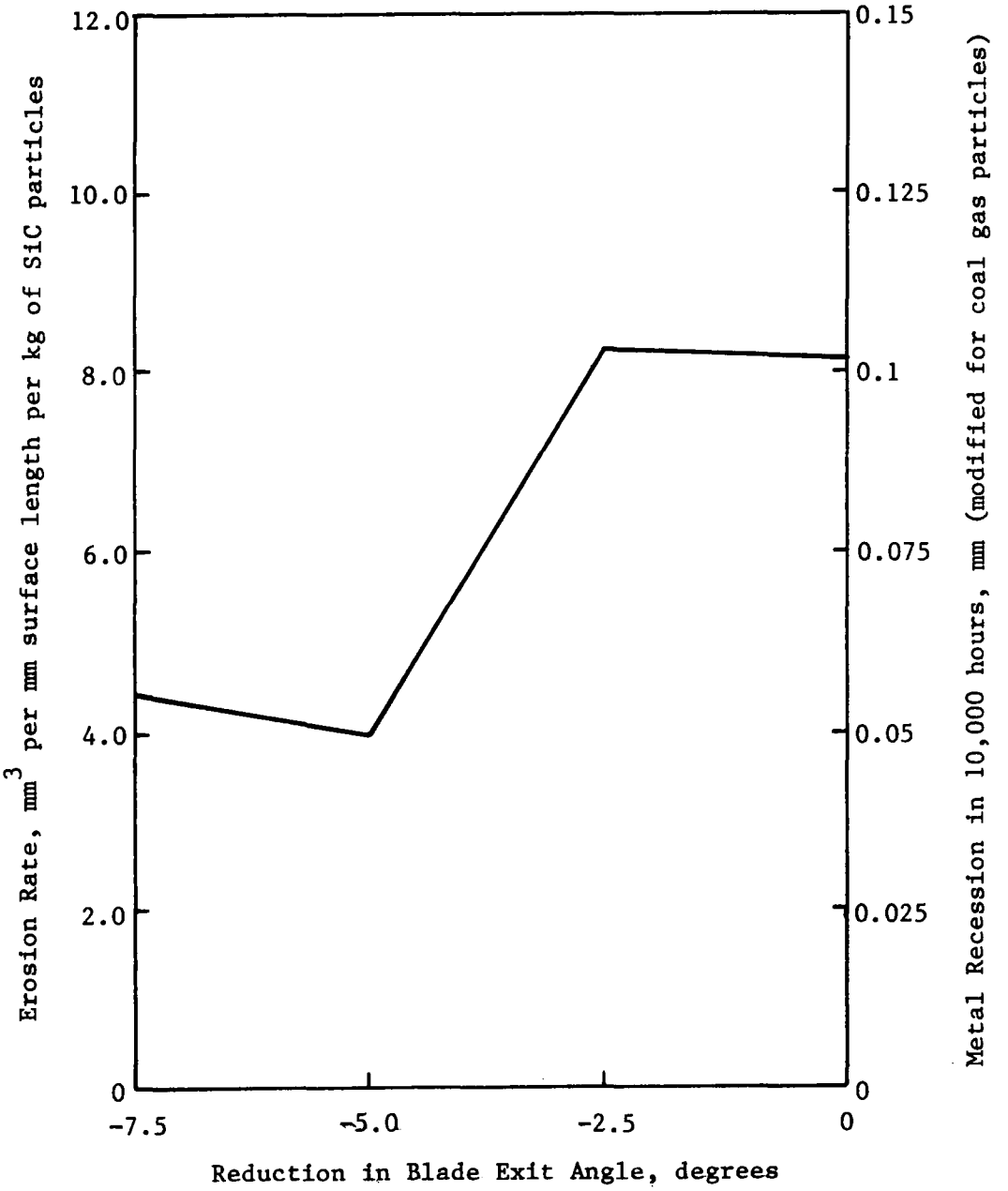

FIG. 17. TRAILING EDGE EROSION OF STATOR AS A FUNCTION OF REDUCTION IN BLADE EXIT ANGLE

Figure 18 shows the effect of changing the leading edge radius on the trailing edge erosion of the stator. It can be seen that a small decrease in the trailing edge erosion occurs when the leading edge radius is reduced. It would have been desirable to determine the erosion for yet smaller radii, however, the erosion program was not capable of this calculation.

The effect of reducing the degree of reaction of the turbine stage on the trailing edge erosion of the stator is shown in Figure 19. As can be seen in the figure, reducing the degree of reaction causes an increase in the trailing edge erosion of the stator. This is because a decrease in the degree of reaction results in an increase in the stator blade exit angle. Increasing the blade exit angle increases the trailing edge erosion as shown in Figure 17.

Rotor

Figure 20 shows the effect of blade exit angle reduction on the trailing edge erosion of the rotor. The results are in close agreement with the stator exit angle variation. Again, greater impact velocities and frequency of impact at higher blade angles caused increases in trailing edge erosion.

The effect of leading edge radius changes on the trailing edge erosion of the rotor is shown in Figure 21. As can be seen in the figure, a large decrease in trailing edge erosion occurs when the leading edge radius is reduced. As can also be seen, a small decrease in trailing edge erosion occurs when the leading edge radius is

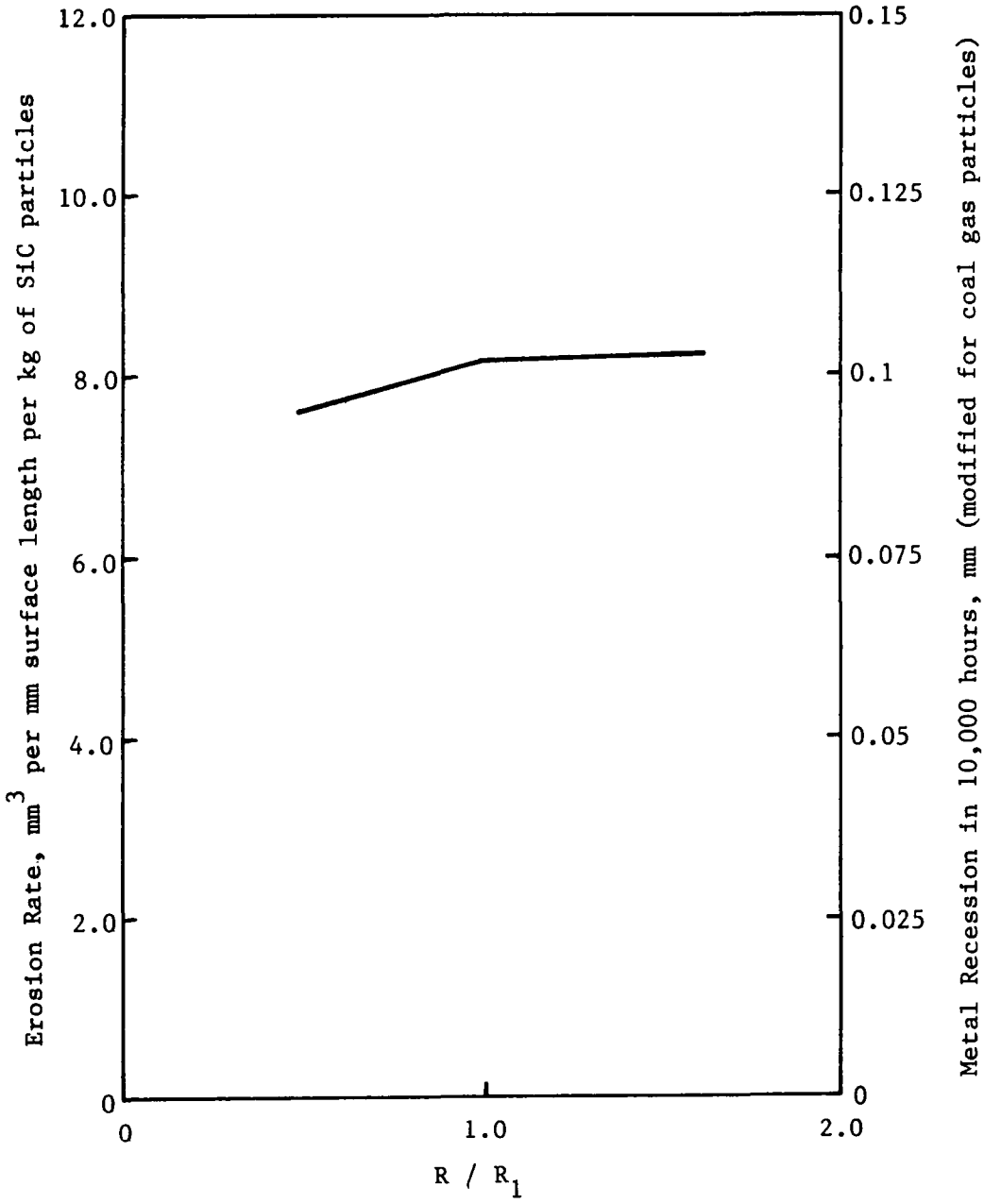

FIG. 18. TRAILING EDGE EROSION OF STATOR AS A FUNCTION OF LEADING EDGE RADIUS

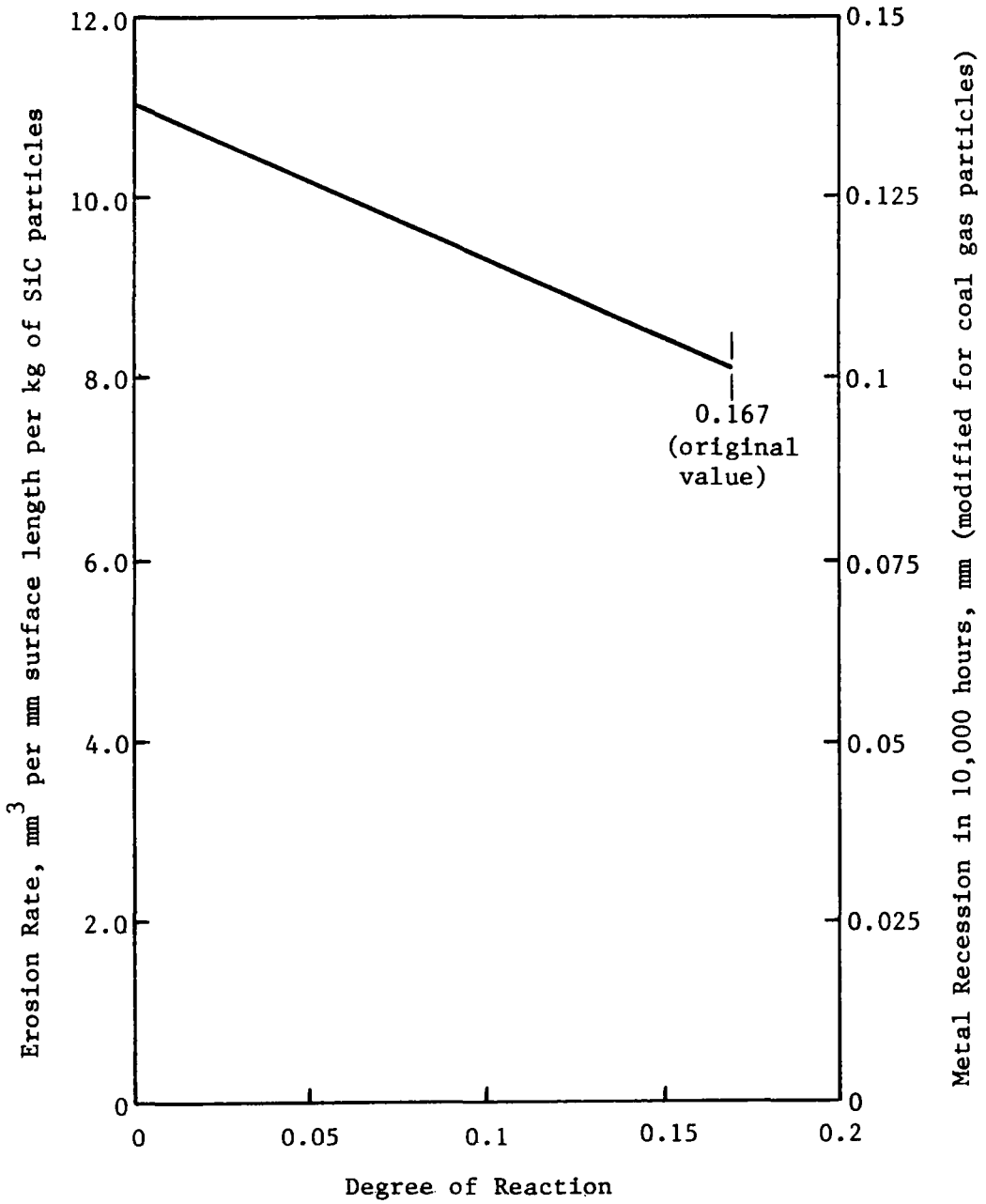

FIG. 19. TRAILING EDGE EROSION OF STATOR AS A FUNCTION OF THE TURBINE STAGE DEGREE OF REACTION

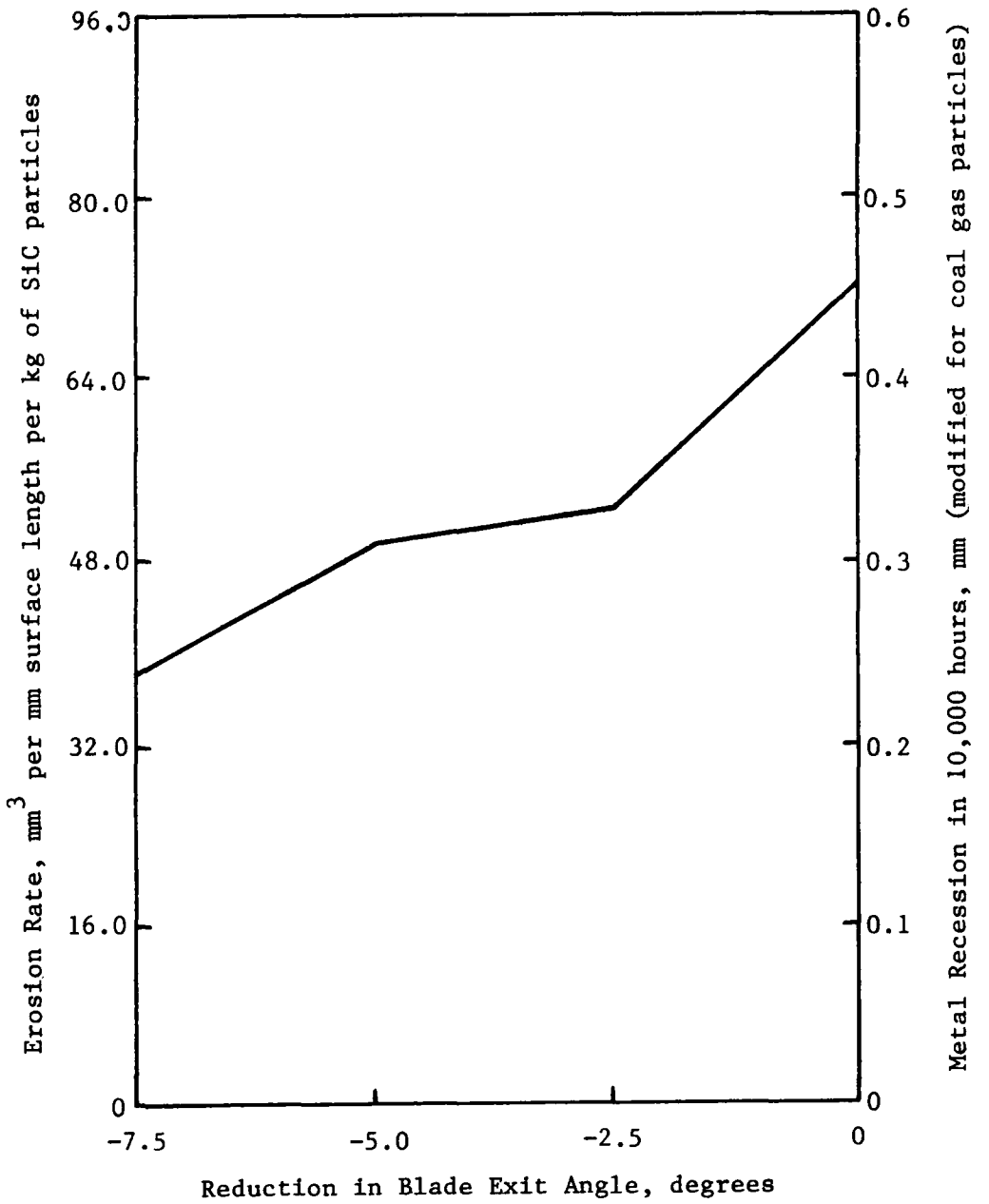

FIG. 20. TRAILING EDGE EROSION OF ROTOR AS A FUNCTION OF REDUCTION IN BLADE EXIT ANGLE

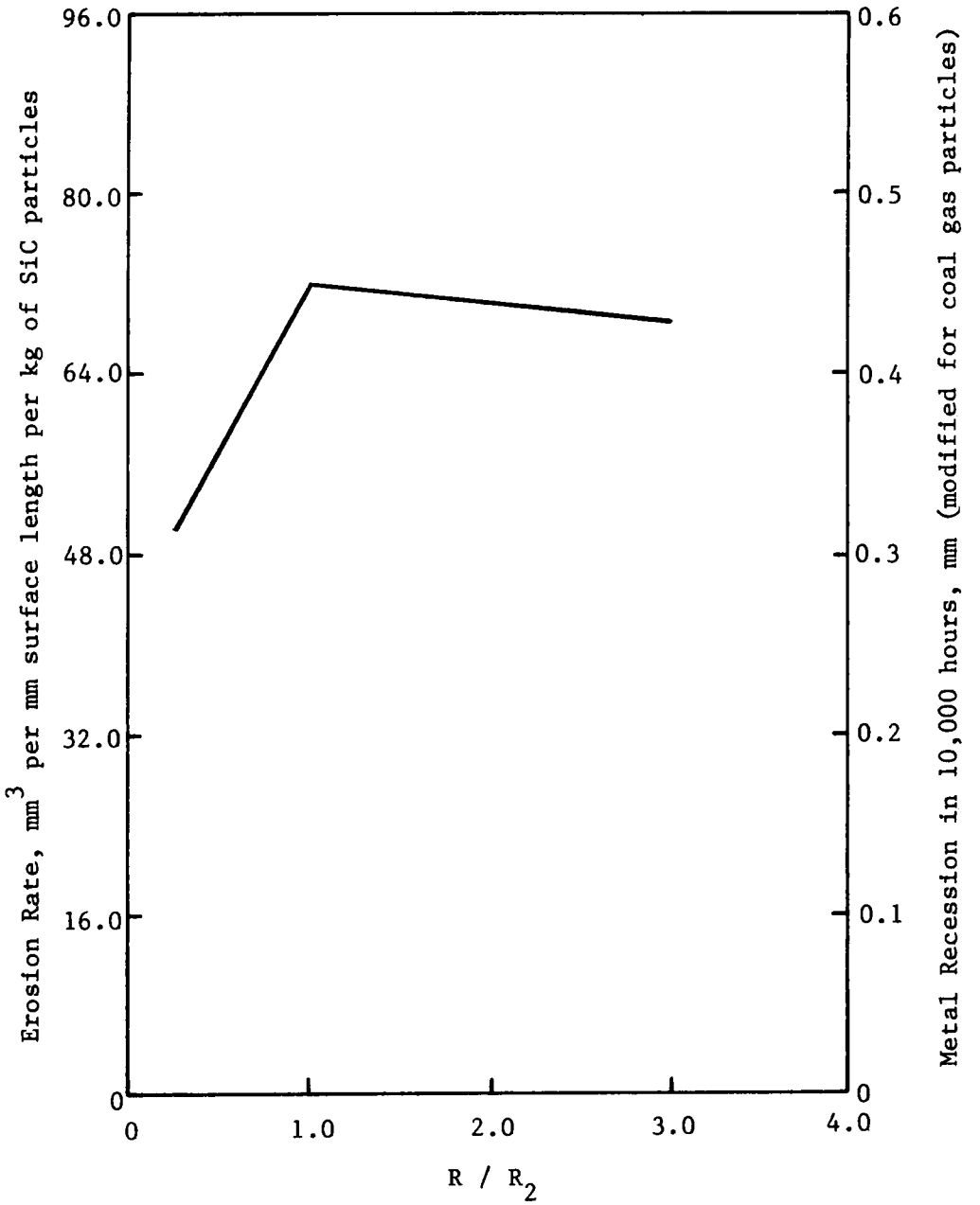

FIG. 21. TRAILING EDGE EROSION OF ROTOR AS A FUNCTION OF LEADING EDGE RADIUS

increased. These variations in leading edge radius are larger than those used for the stator. It may be that a larger decrease or increase in the leading edge radius of the stator would have yielded similar results.

The effect of reducing the degree of reaction of the turbine stage on the leading and trailing edge erosion of the rotor is shown in Figure 22. As can be seen, the trailing edge erosion of the rotor is decreased as the degree of reaction is reduced. This is because reducing the degree of reaction results in lower relative velocities at the rotor exit. The leading edge erosion, however, is increased as the degree of reaction is reduced. This is due to the higher relative velocities at the rotor inlet when the degree of reaction is reduced.

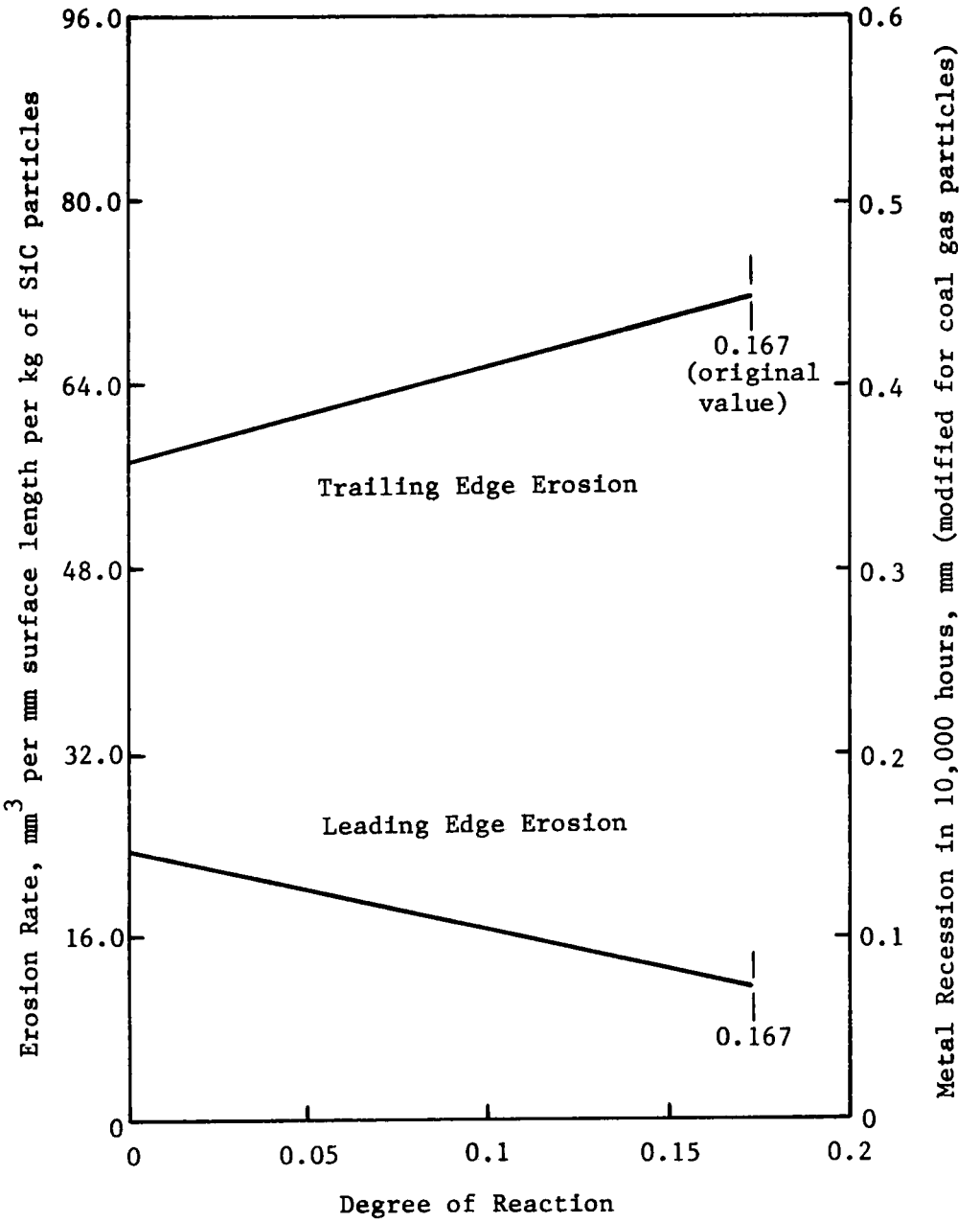

FIG. 22. LEADING AND TRAILING EDGE EROSION OF ROTOR AS A FUNCTION OF THE TURBINE STAGE DEGREE OF REACTION

XII. CONCLUSIONS

The following conclusions can be made from the blade profile variation investigation over the range of parameters studied:

1. Trailing edge erosion is decreased in both the rotor and stator when the blade exit angle is reduced.
2. Decreasing the blade leading edge radius results in a decrease in trailing edge erosion in both the rotor and stator. Increasing the blade leading edge radius results in a small decrease in trailing edge erosion in the rotor.
3. Reducing the degree of reaction of the turbine stage causes a shift in the erosion levels at critical blade stations. When the degree of reaction is reduced to zero, the stator trailing edge erosion and rotor leading edge erosion are increased while the rotor trailing edge erosion is decreased.

XIII. RECOMMENDATIONS FOR FUTURE WORK

1. The erosion rates predicted in this investigation should be extended and compared with experimentally determined erosion rates from references 19 or 26.

2. The effect of inlet gas velocity on the blade erosion should be determined.

3. The erosion model should be extended to include deposition and corrosion.

4. The erosion characteristics of coal ash particles under conditions representative of turbine passages should be experimentally determined.

XIV. REFERENCES

1. Menguturk, M., and Sverdrup, E. F., "Tolerance of a Large Electric Utility Turbine to Erosion Damage by Coal Ash Particles", Westinghouse Research and Development Center, Pittsburgh, PA, ASTM Symposium on Erosion, Vail, Colo., October, 1977.

2. Yellott, J. I., "An Experimental Coal-Burning Gas Turbine", Midwest Power Conference, Locomotive Development Committee, Bituminous Coal Research, Inc., Chicago, Illinois, April, 1950.

3. Yellott, J. I., P. R. Broadley, and D. Buckley, "Progress Report on the Coal-Burning Gas Turbine", Midwest Power Conference, Locomotive Development Committee, Bituminous Coal Research, Inc., Chicago, Illinois, April, 1951.

4. Yellott, J. I., P. R. Broadley and D. Buckley, "First 1000 Hr of Coal-Burning Gas-Turbine Tests", Power, June, 1951.

5. Yellott, J. I., and P. R. Broadley, "Annual Report to the Locomotive Development Committee of Bituminous Coal Research, Inc.", covering the period May 1, 1950, to April 30, 1951, The Locomotive Development Committee of Bituminous Coal Research, Inc., June, 1951.

6. Broadley, P. R., and W. M. Meyer, "Direct-Fired Coal-Burning Gas-Turbine Operations", Conference on Coal-Burning Gas Turbines, McGill University, Montreal, Quebec, November, 1956.

7. Yellott, J. I., and P. R. Broadley, "Progress Report on Preliminary Tests of a 4250 Horsepower Coal-Burning Locomotive-Type Gas Turbine Power Plant", American Power Conference, Locomotive Development Committee, Bituminous Coal Research, Inc., Chicago, Illinois, March, 1952.

8. Yellott, J. I., and P. R. Broadley, "Photographic Report Number 51-2", Mechanical Advisory Group, Locomotive Development Committee, Bituminous Coal Research, Inc., December, 1951.

9. Yellott, J. I., and P. R. Broadley, "Progress Continues on Coal-Burning Gas Turbine Plant", Power Engineering, June, 1953.

10. Yellott, J. I., P. R. Broadley and W. M. Meyer, "Acceptance and Operational Tests of a 4250 HP Coal-Burning Gas Turbine, I--Preliminary Oil-Fired Operation", Gas Turbine Power Division Fall Meeting, Milwaukee, Wisconsin, ASME Paper 54-F-39, September, 1954.

11. Yellott, J. I., P. R. Broadley and W. M. Meyer, "Acceptance and Operational Tests of a 4250 HP Coal-Burning Gas Turbine, Part II--Coal-Fired Operation", Gas Turbine Power Division Fall Meeting, Milwaukee, Wisconsin, ASME Paper No. 54-F-40, September, 1954.

12. Yellott, J. I., "Report on 750 Hour Test of 4250 Horsepower Coal-Fired Gas Turbine Power Plant", Locomotive Development Committee, Bituminous Coal Research, Inc., September, 1952.

13. Yellott, J. I., et al, "Photographic Report Number 54-1, 300 Hour Test on 4250 HP Coal-Burning Gas Turbine", Locomotive Development Committee, Bituminous Coal Research, Inc., September, 1954.

14. Yellott, J. I., P. R. Broadley and W. M. Meyer, "Technical Supplement, The Progress of the LDC--Alco Coal-Burning Gas Turbine Project during the Period from October 1, 1954 to September 1, 1955, 1955 Annual Report to the Locomotive Development Committee of Bituminous Coal Research, Inc., Bituminous Coal Research Inc., September, 1955.

15. Yellott, J. I., P. R. Broadley and W. M. Meyer, "Summary of Operation of the LDC--Alco Coal-Burning Gas Turbine Project", October 1, 1954, to September 1, 1955, Summary of 1955 Operation, Bituminous Coal Research, Inc., September, 1955.

16. Yellott, Y. I., "Annual Report, 1957", The Locomotive Development Committee of Bituminous Coal Research, Inc., Dunkirk, NY, 1957.

17. McGee, J. P. and R. C. Corey, "Bureau of Mines Coal Fired Gas Turbine Research Project", Combustion, April, 1960, pp. 67-72.

18. McGee, J. P. and R. C. Corey, "Redesign and Assembly of Turbine", United States Department of the Interior, Bureau of Mines, Report of Investigations No. 5958, 1962.

19. Smith, J. and W. L. Simpson, "Test of New Turbine Blade Design", United States Department of the Interior, Bureau of Mines, Report of Investigations No. 6920, 1967.

20. Cargill, R. W. and W. L. Tennyson, "Coal Fired Gas Turbine Completes Run With New Blades", Power Engineering, May, 1964, pp. 47-48.

21. Nabors, W. M., "Bureau of Mines Progress in Developing the Coal-burning Gas Turbine Power Plant", Journal of Engineering for Power, Transactions of the ASME, April, 1965, pp. 215-221.

22. Joseph, J., "Union Pacific's Coal-burning Gas Turbine-Electric Locomotive", Diesel and Gas Engine Progress, Apr., 1963, pp. 56-57.

23. Morris, R. I., "New Developments in Coal are Leading to New Developments in Coal Fired Gas Turbine", Railway Age, Aug. 5, 1957, pp. 20-23.

24. Fraas, A. P., "Survey of Turbine Bucket Erosion, Deposits, and Corrosion", ASME Paper No. 75-GT-123, March, 1975.

25. Wisdom, J. C., "Brown Coal Burning Gas Turbines", The Engineer Aug. 29, 1958, pp. 328-331.

26. Aeronautical Research Laboratories, "Report of the Inter-departmental Steering Committee, The Coal Burning Gas Turbine Project", Australian Government Publishing Service, Canberra, 1973.

27. Morley, W. J., "Brown Coal Ash Deposition in the Open-cycle Gas Turbine", Journal of the Institute of Fuel, May, 1964, pp. 187-200.

28. Mordell, D. L., "Indirect-fired Gas Turbines", The Engineer, February 1957, pp. 210-213.

29. Mordell, D. L. and K. T. Tyndall, "Test of an Experimental Coal-burning Turbine", Transactions of the ASME, November 1956, pp. 1807-1821.

30. Mordell, D. L., Conference on Coal Burning Gas Turbines, Proceedings, McGill University, Montreal, Quebec, 1956.

31. Finnie, I., "The Mechanism of Erosion of Ductile Metals," Proc. 3rd U.S. National Congress of Applied Mechanics, 1958, pp. 527-532.

32. Finnie, I., "Erosion of Surfaces by Solid Particles", Wear, 3, 1960.

33. Bitter, J.G.A., "A Study of Erosion Phenomena", Part I, Wear, 6, 1963, 5-21.

34. Bitter, J.G.A., "A Study of Erosion Phenomena", Part II, Wear, 6, 1963, 169-190.

35. Neilson, J. H. and A. Gilchrist, "Erosion by a Stream of Solid Particles", Wear, 11, 1968, 111-122.

36. Head, W. J. and M. E. Harr, "The Development of a Model to Predict the Erosion of Materials by Natural Contaminants", Wear, 15, 1970.

37. Grant, G., A Model to Predict Erosion in Turbomachinery Due to Solid Particles in Particulated Flow, University of Cincinnati, Ph.D. Thesis, 1973.

38. Tabakoff, W. and M. F. Hussein, "Effect of Suspended Solid Particles on the Properties in Cascade Flow", AIAA Journal, Vol. 9, No. 8, August 1971.

39. Grant, G., R. Ball and W. Tabakoff, "An Experimental Study of the Erosion Rebound Characteristics of High Speed Particles Impacting a Stationary Specimen", University of Cincinnati Technical Report 73-36, Cincinnati, Ohio, May 1973.

40. Tabakoff, W., G. Grant, and R. Ball, "An Experimental Investigation of Certain Aerodynamic Effects on Erosion", AIAA Paper No. 74-639, July 1974.

41. Tabakoff, W., W. Hosny, and A. Hamed, "Effect of Solid Particles on Turbine Performance", ASME Paper No. 75-GT-41, March 1975.

42. Tabakoff, W., W. Hosny, and A. Hamed, "Performance and Flow Properties Change Through a Rocket Turbine by Presence of Solid Particles", Astronautica Acta, Vol. 18, 1974.

43. Tabakoff, W. and M. Hussein, "Properties and Particle Trajectories of Gas-Particle Flows in Cascades", Department of Aerospace Engineering, University of Cincinnati, Cincinnati, Ohio, 1972.

44. Hussein, M., The Dynamic Characteristics of Solid Particulates in Rotating Turbomachinery", Ph.D. Dissertation, University of Cincinnati, 1972.

45. Clevenger, W. B. and W. Tabakoff, "The Dynamics of Atmospheric Dust Particles in Aircraft Auxilary Power Radial Inflow Turbines", AIAA Paper No. 75-844, June 1975.

46. Clevenger, W. B. and W. Tabakoff, "Erosion in Radial Inflow Turbines - Volumes I, II, III, IV and V", University of Cincinnati, Department of Aerospace Engineering: Vol. I - NASA CR 134589, February 1974; Vol. II - NASA CR 134616, April 1974; Vol. III - NASA CR 134700, August 1974; Vol. IV - NASA CR 134677, January 1975; Vol. V - NASA CR 134787, May 1975.

47. Grant, G. and W. Tabakoff, "Erosion Prediction in Turbomachinery Resulting from Environmental Solid Particles", Journal of Aircraft, Vol. 12, No. 5, May 1975.

48. Ulke, A., An Approximate Analysis of the Effect of Secondary Flows on the Motion of Particulates in an Axial Flow Gas Turbine, Ph.D. Dissertation, Carnegie Mellon University, 1975.

49. Dubberley, J., An Analytical Parameter Study on the Erosion of Turbine Blades Subjected to Flow Containing Particulates, M.S. Thesis, Virginia Polytechnic Institute and State University, 1977.

50. Katsanis, T., "Fortran Program for Calculating Transonic Velocities on a Blade-to-Blade Stream Surface of a Turbomachine", NASA TN D-5427, 1969.

51. Ainley, D., "The Performance of Axial-flow Turbines", Internal Combustion Turbines, ASME, 1949.

52. Cohen, H., G. F. C. Rogers, H. I. H. Saravanamutto, Gas Turbine Theory, Second Edition, Halsted Press, John Wiley, New York, 1974.

53. Baumgarter, F. and R. Ansler, "Presentation of a Blade-Design Method for Axial-Flow Turbines, Including Design and Test Results of a Typical Axial-Flow Stage", Journal of Engineering for Power, Transactions of the ASME, January 1960, pp. 19-26.

54. Pinkerton, R., "Effect of Nose Shape on the Characteristics of Symmetrical Airfoils", NACA TN 386.

55. Jacobs, E., K. Ward, and R. Pinkerton, "The Characteristics of 78 Related Airfoil Sections from Tests in the Variable-density Wind Tunnel", NACA TR 460.

56. Smeltzer, C., and P. Sage, "Mechanisms of Metal Removal by Impacting Dust Particles", Transactions of the ASME, Journal of Basic Engineering, September 1970, pp. 639-654.

XV. APPENDICES

APPENDIX A. DETERMINATION OF METAL RECESSION DUE TO COAL ASH PARTICLES FROM THE EROSION RATE OF SiC PARTICLES

The erosion rate, $mm^3/mm\text{-}kg$, of SiC particles is obtained directly from the output of the erosion model. To obtain the metal recession in 10,000 hours due to coal ash particles it is necessary to assume an inlet particle concentration of 2×10^{-7} kilograms per kilogram of expansion gas.

The mass flow rate through the Model 501B turbine is 308 kg/sec. There are 48 stator and 95 rotor blades in the first stage. Using this information, the total mass of particles passing through each blade channel in 10,000 hours is found. The total particle mass passing through each stator channel is 41.9 kg; the total particle mass passing through each rotor channel is 21.1 kg.

The blade heights of the first stage stator and rotor blades are 131 mm and 102 mm, respectively. Coal ash particles are assumed to be 1/25 as erosive as SiC particles (26). Metal recession is then calculated by multiplying the erosion rate by the total particle mass through the channel and dividing by the blade height times 25.

APPENDIX B. EROSION PLOTS

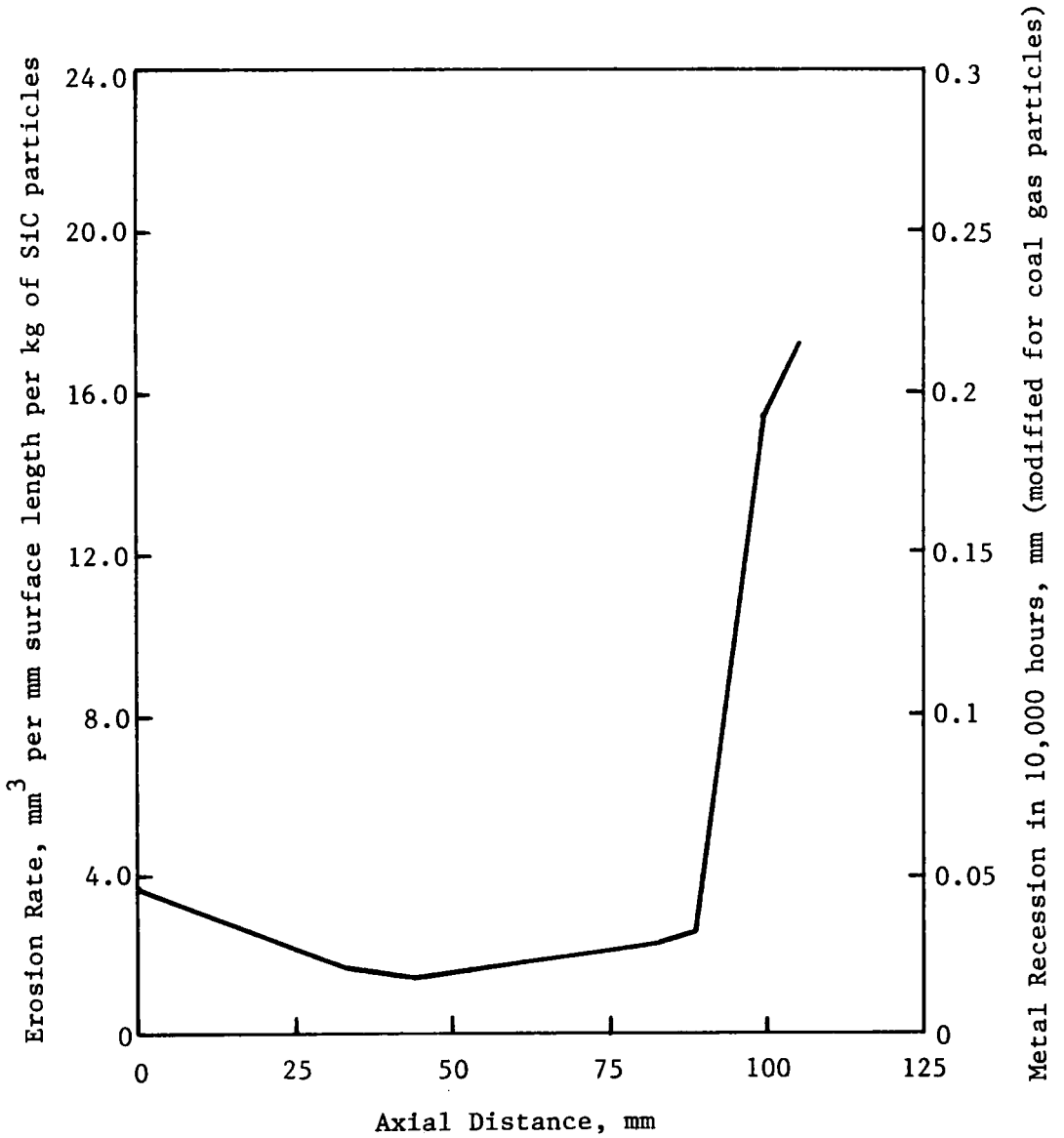

FIG. B-1. STATOR - BLADE EXIT ANGLE REDUCED 2.5°, EROSION RATE AS A FUNCTION OF AXIAL POSITION

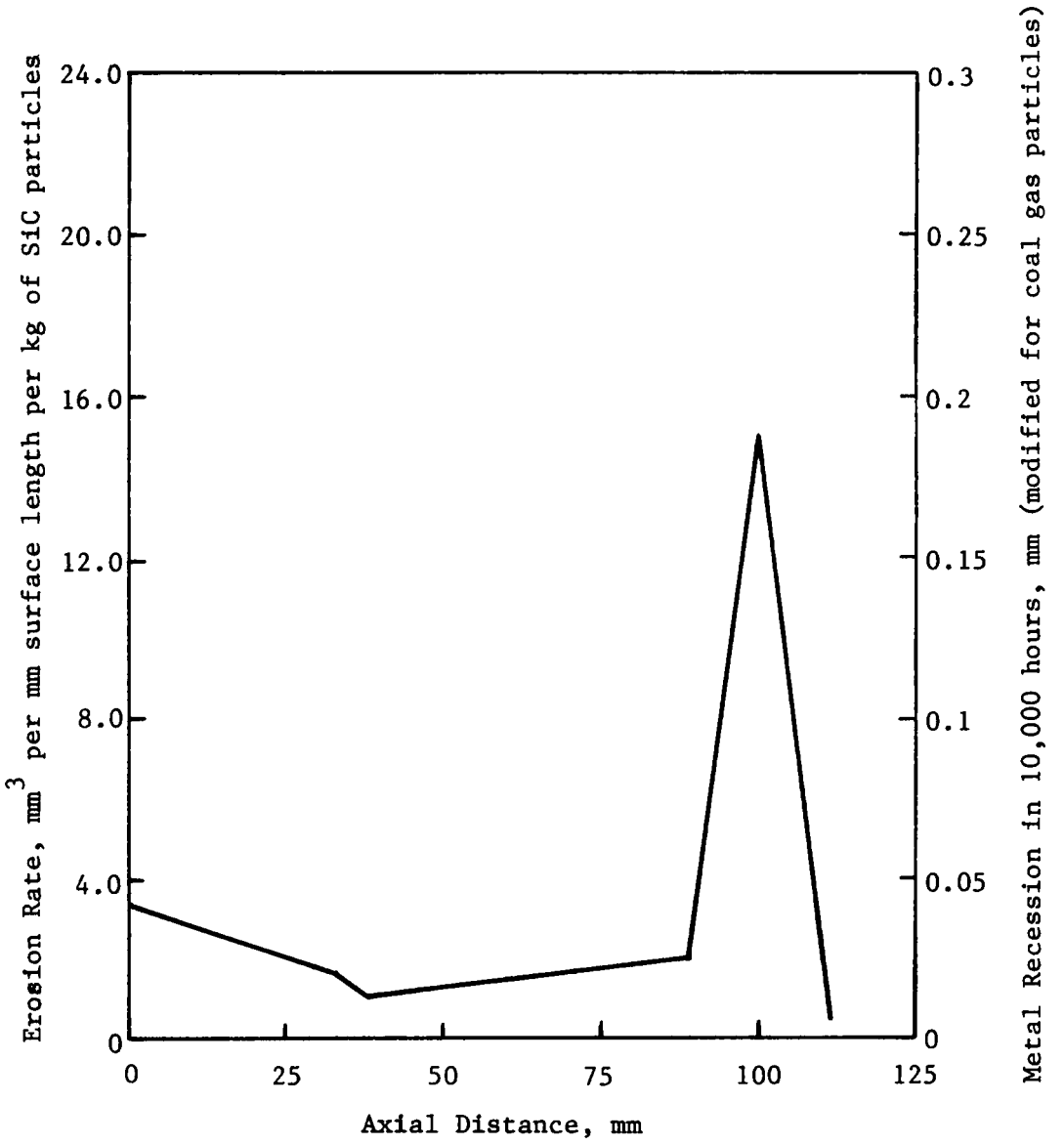

FIG. B-2. STATOR - BLADE EXIT ANGLE REDUCED 5.0°, EROSION RATE AS A FUNCTION OF AXIAL POSITION

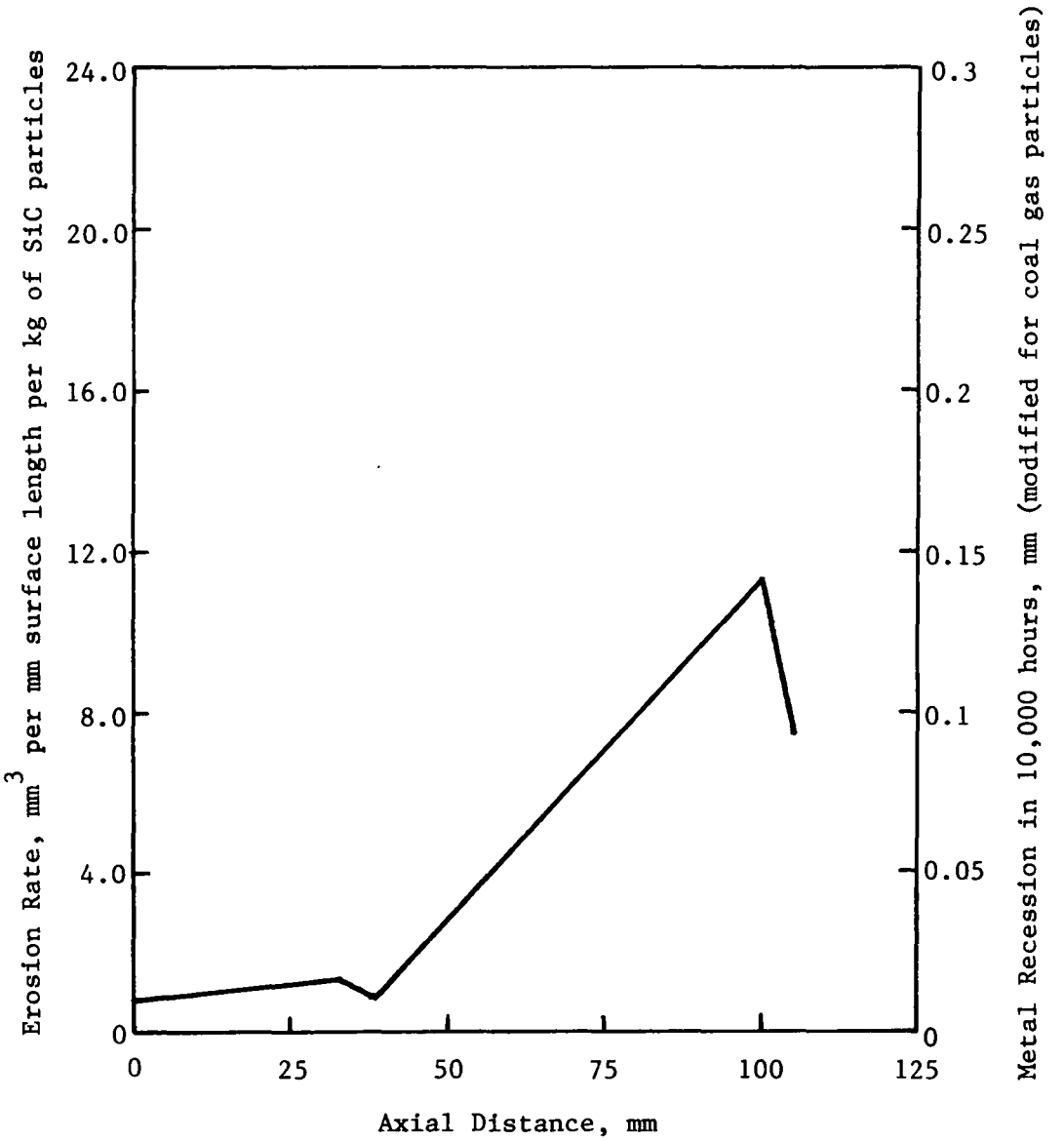

FIG. B-3. STATOR - BLADE EXIT ANGLE REDUCED 7.5°, EROSION RATE AS A FUNCTION OF AXIAL POSITION

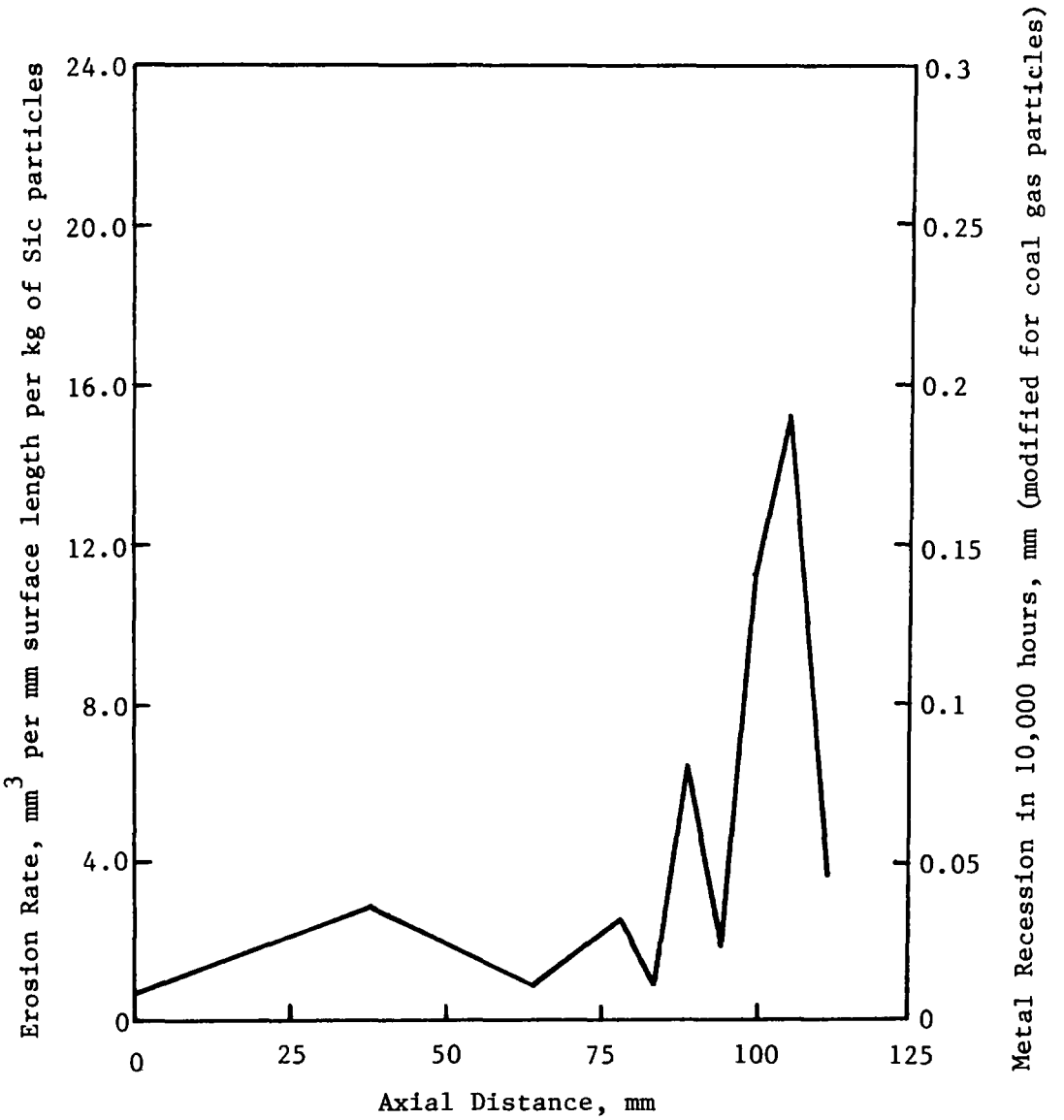

FIG. B-4. STATOR - LEADING EDGE RADIUS = ½ R_1, EROSION RATE AS A FUNCTION OF AXIAL POSITION

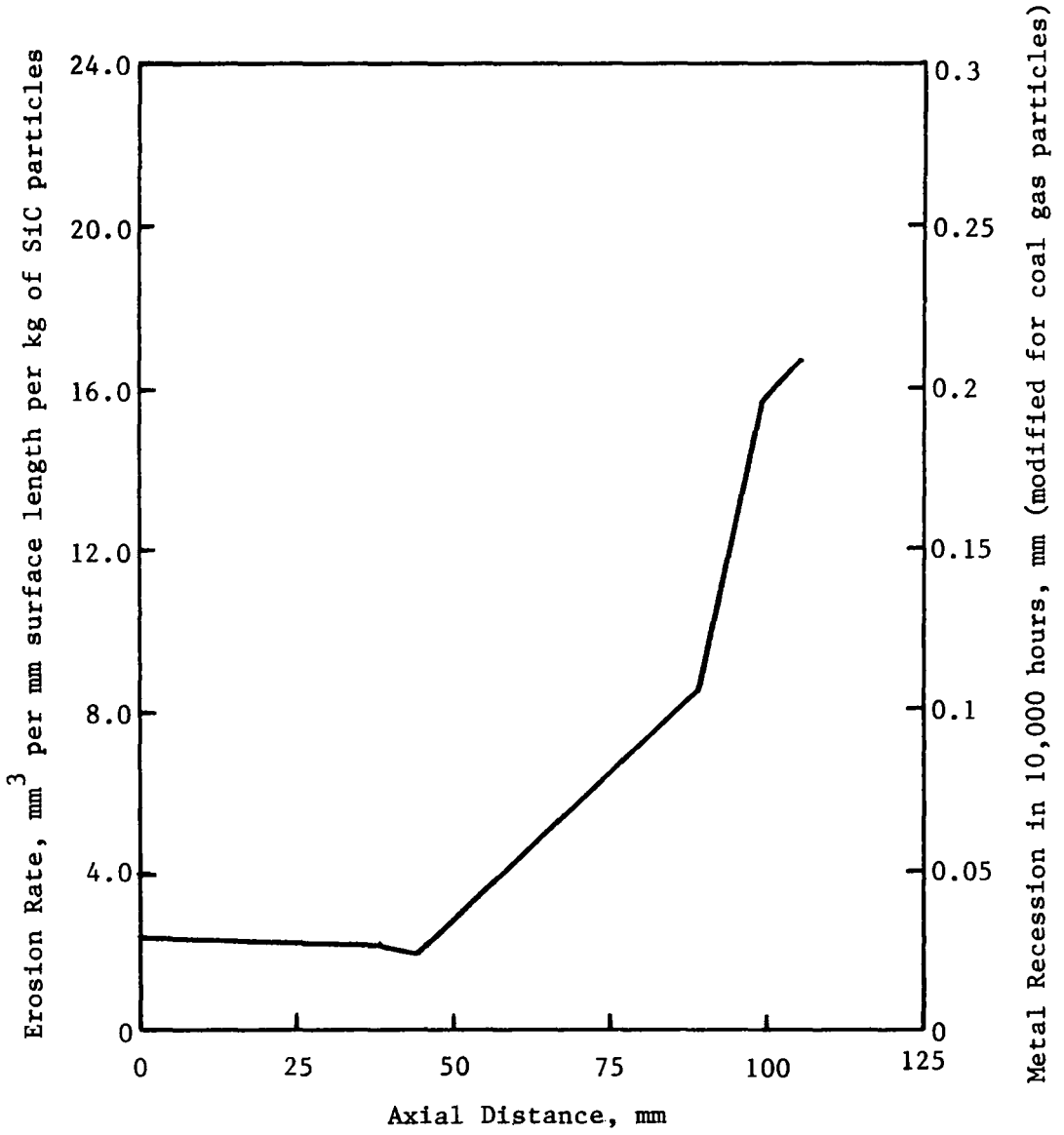

FIG. B-5. STATOR - LEADING EDGE RADIUS = 1.67 R_1, EROSION RATE AS A FUNCTION OF AXIAL POSITION

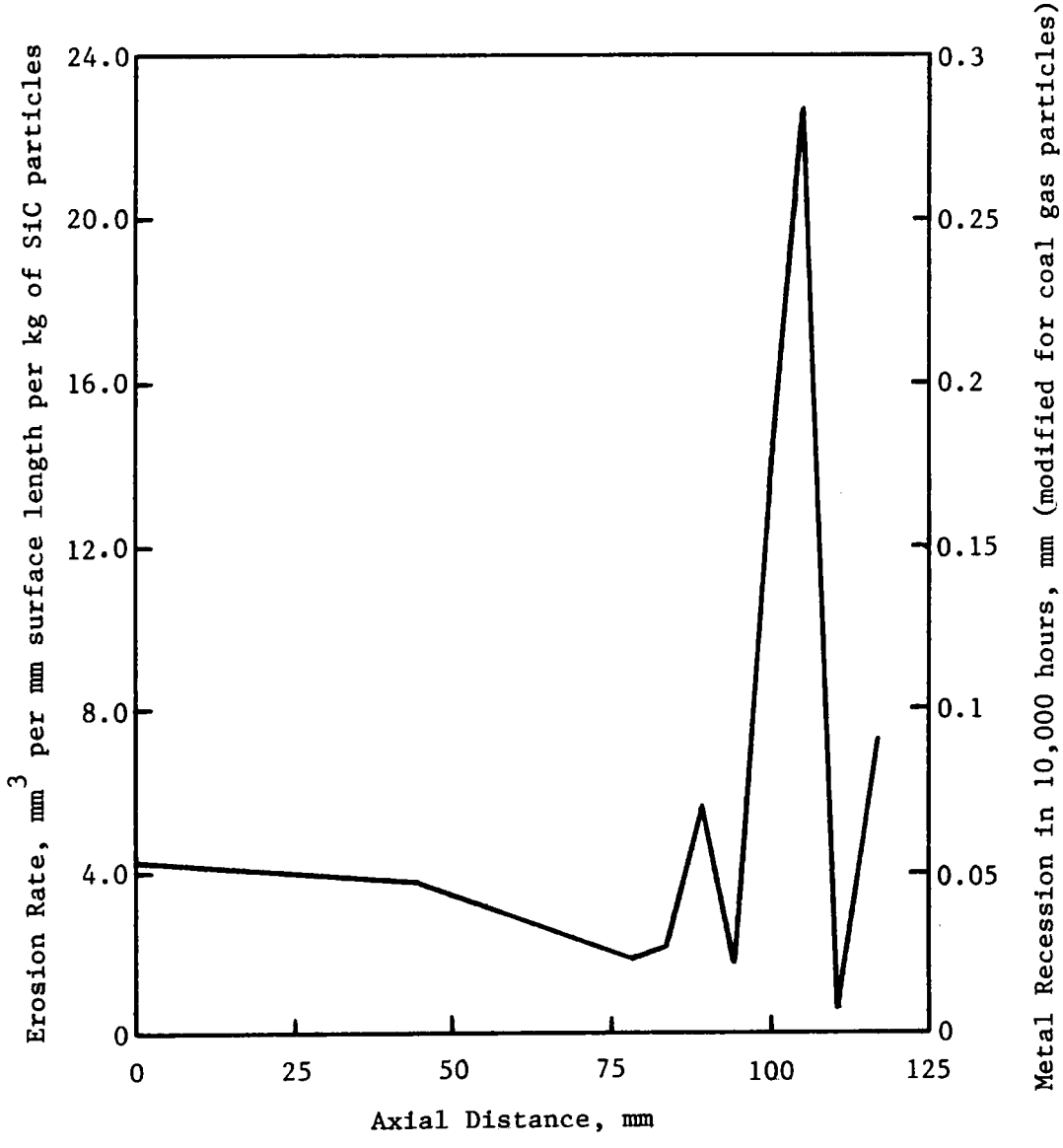

FIG. B-6. STATOR - Λ = 0, EROSION RATE AS A FUNCTION OF AXIAL POSITION

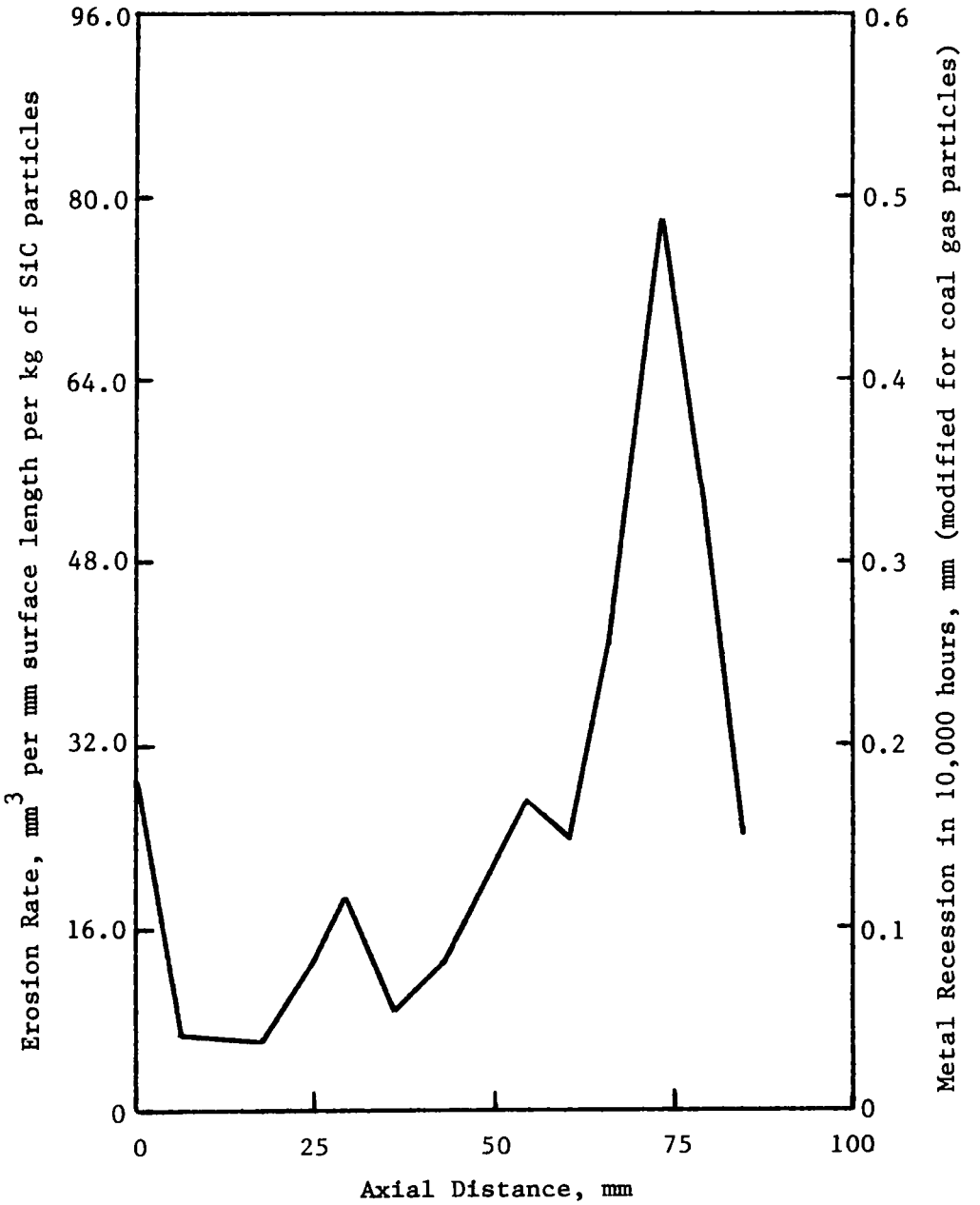

FIG. B-7. ROTOR - BLADE EXIT ANGLE REDUCED 2.5°, EROSION RATE AS A FUNCTION OF AXIAL POSITION

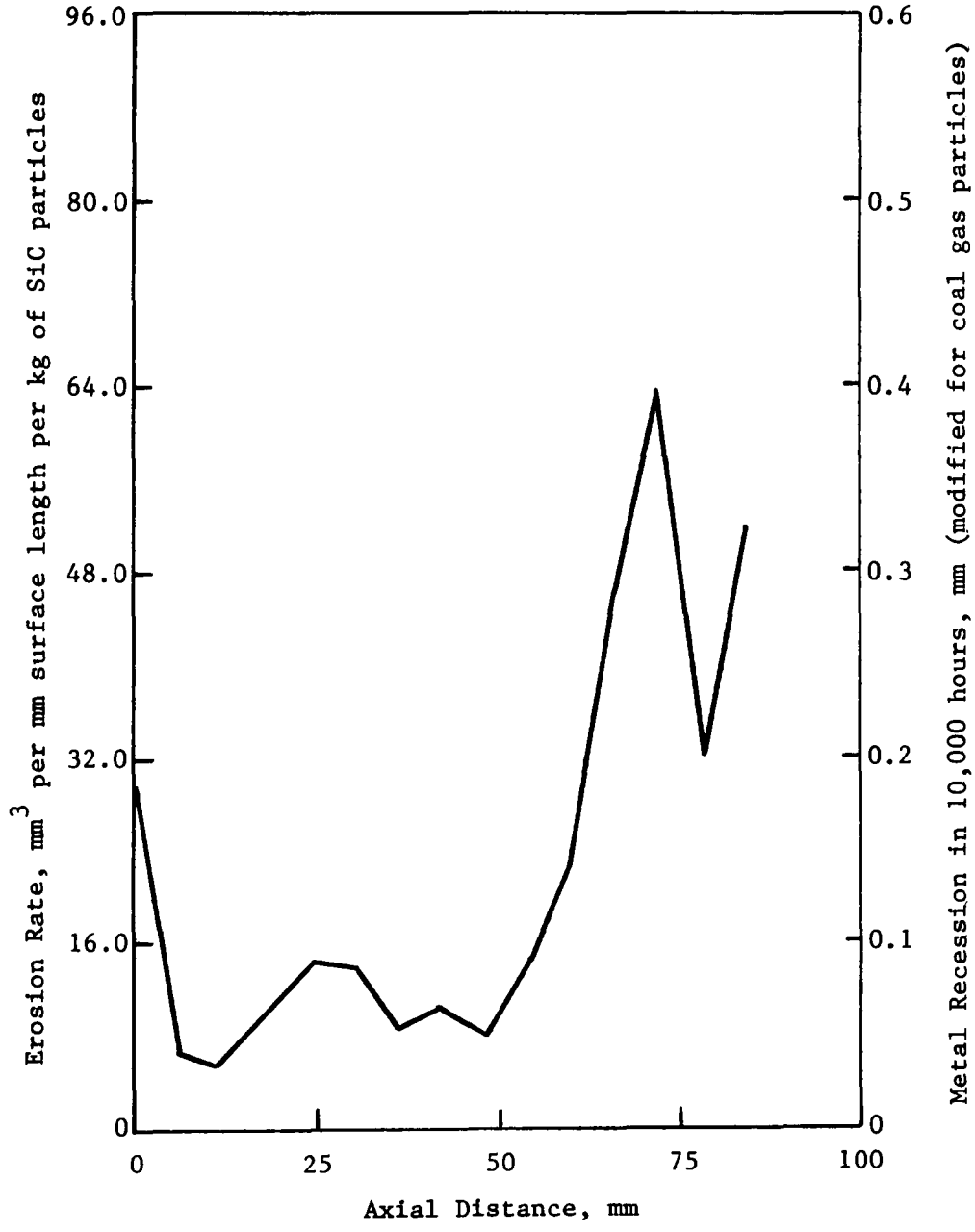

FIG. B-8. ROTOR - BLADE EXIT ANGLE REDUCED 5.0°, EROSION RATE AS A FUNCTION OF AXIAL POSITION

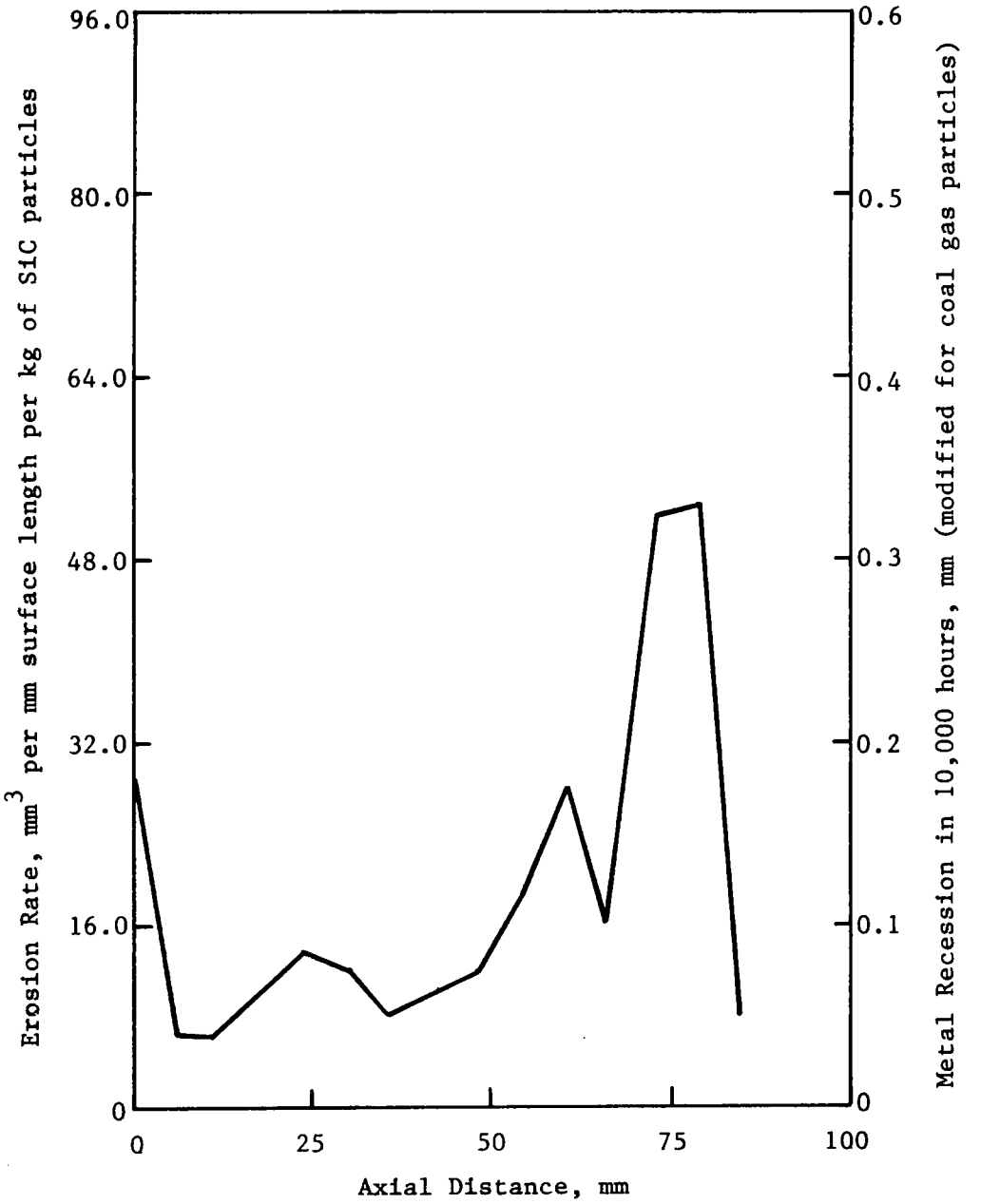

FIG. B-9. ROTOR - BLADE EXIT ANGLE REDUCED 7.5°, EROSION RATE AS A FUNCTION OF AXIAL POSITION

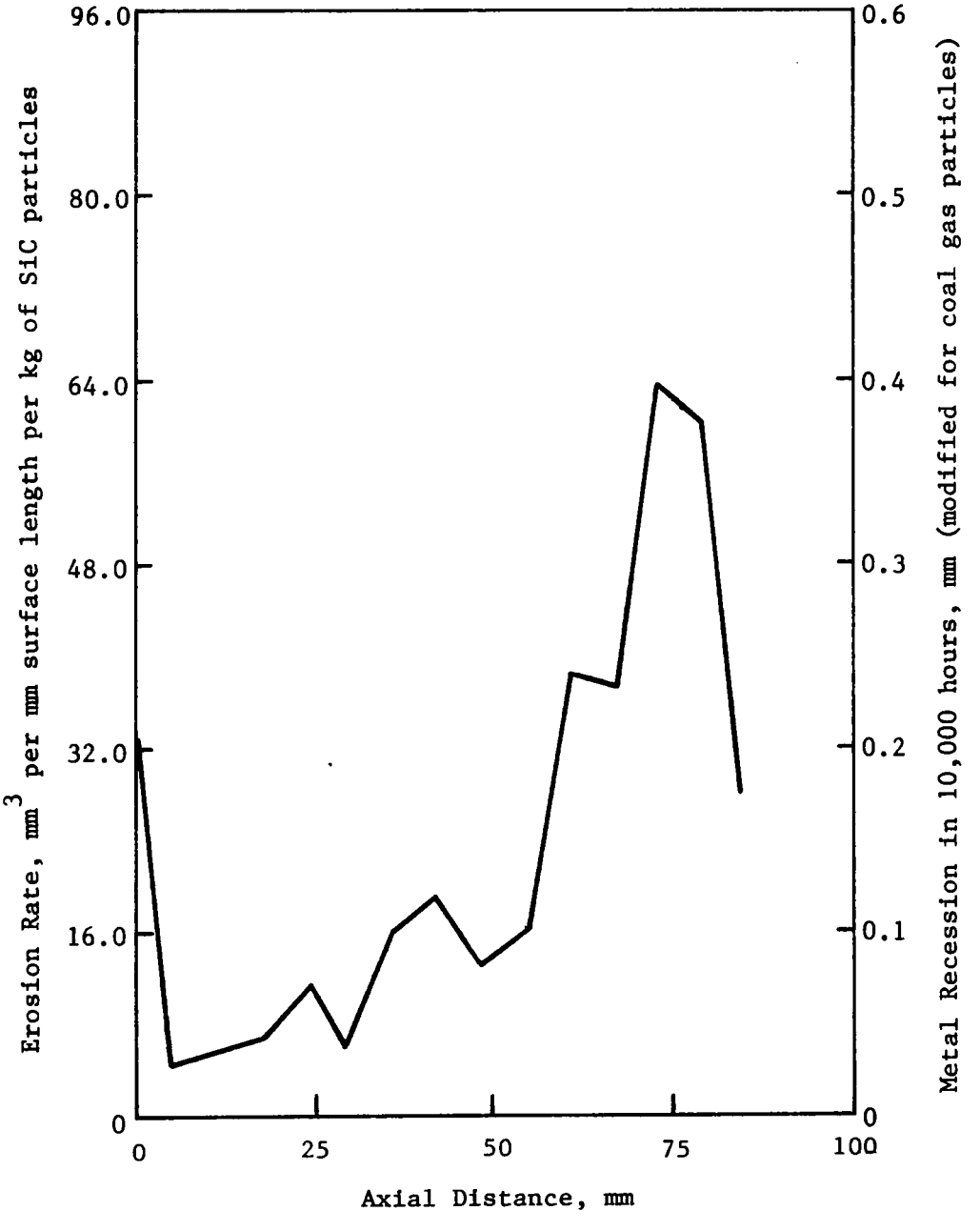

FIG. B-10. ROTOR - LEADING EDGE RADIUS = ¼ R_2, EROSION RATE AS A FUNCTION OF AXIAL POSITION

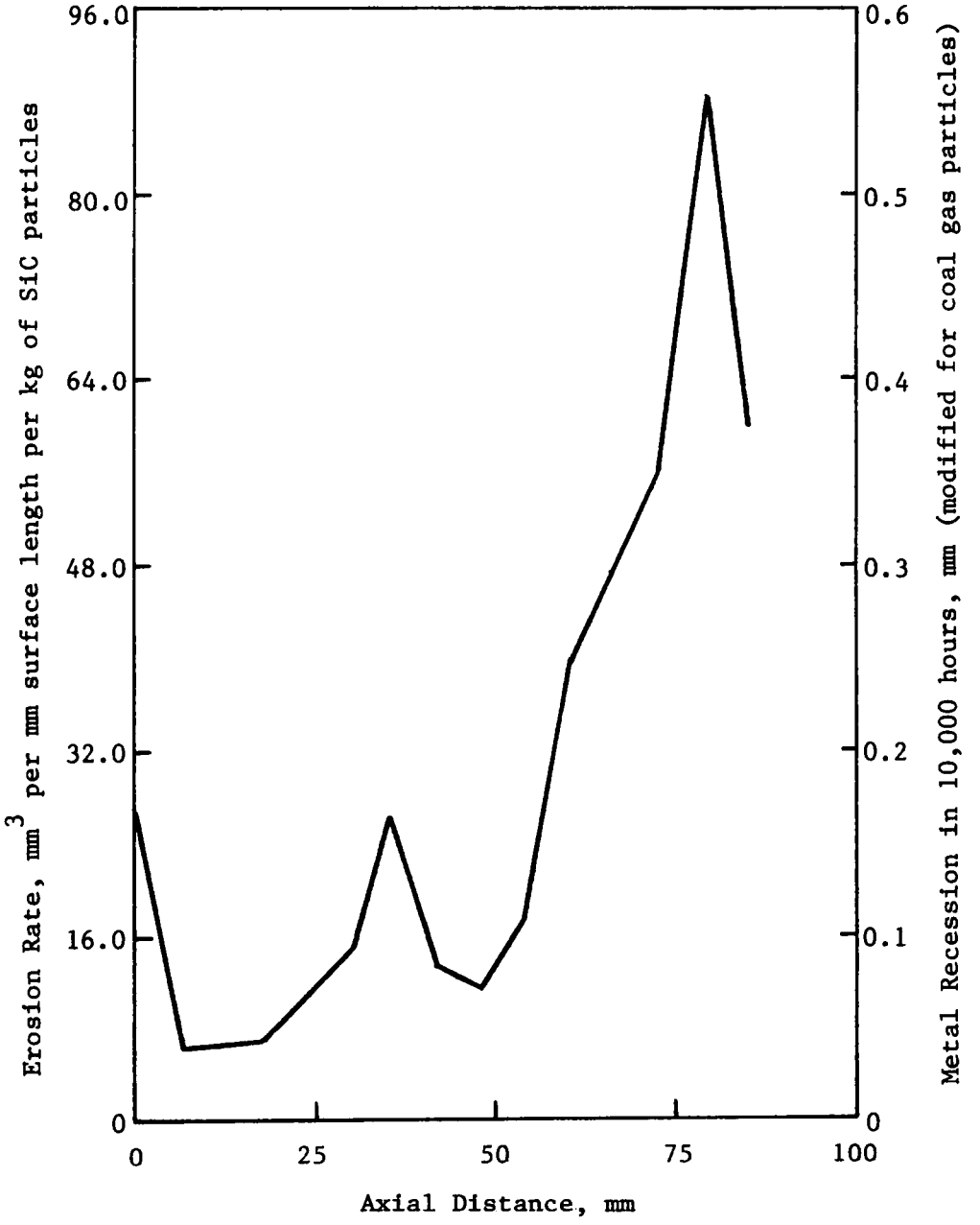

FIG. B-11. ROTOR – LEADING EDGE RADIUS = 3 R_2, EROSION RATE AS A FUNCTION OF AXIAL POSITION

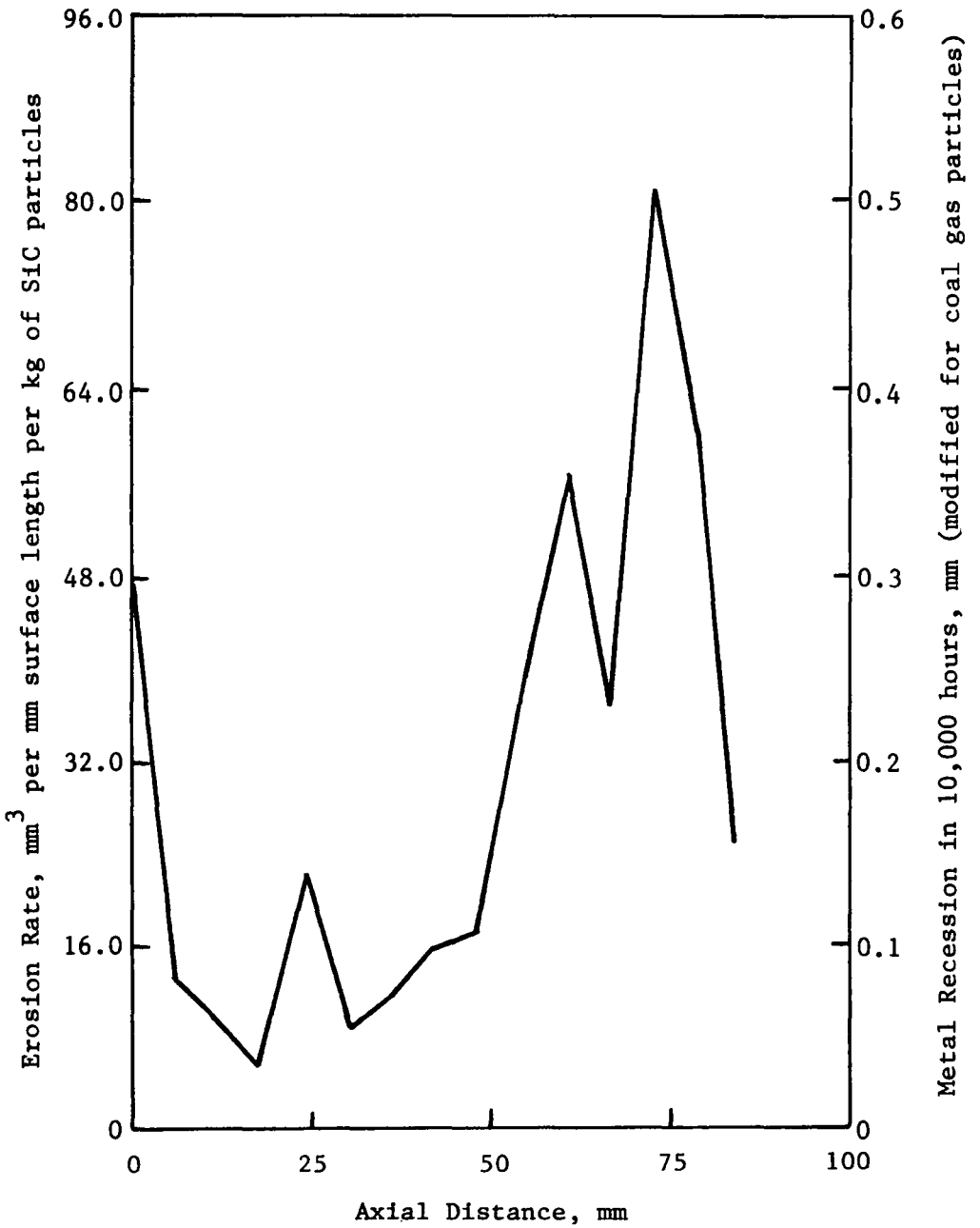

FIG. B-12. ROTOR - Λ = 0, EROSION RATE AS A FUNCTION OF AXIAL POSITION

APPENDIX C. PARTICLE TRAJECTORY PLOTS

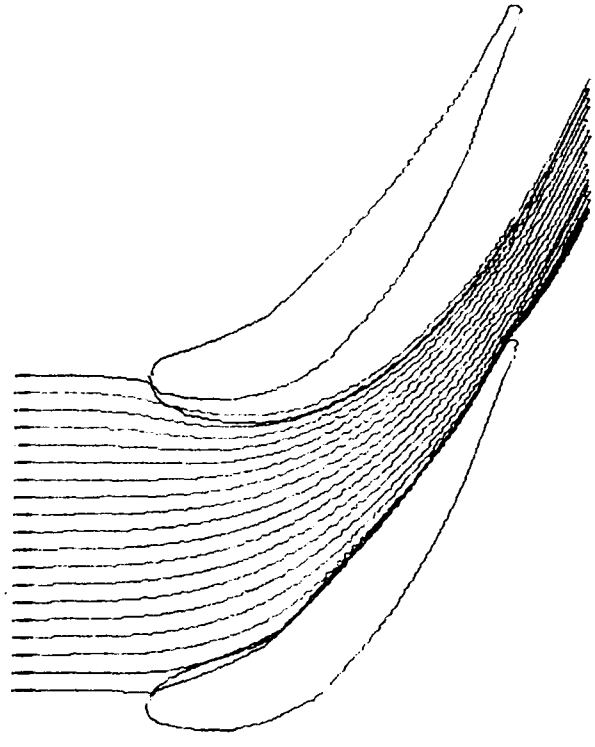

FIG. C-1. WESTINGHOUSE STATOR, PARTICLE TRAJECTORIES

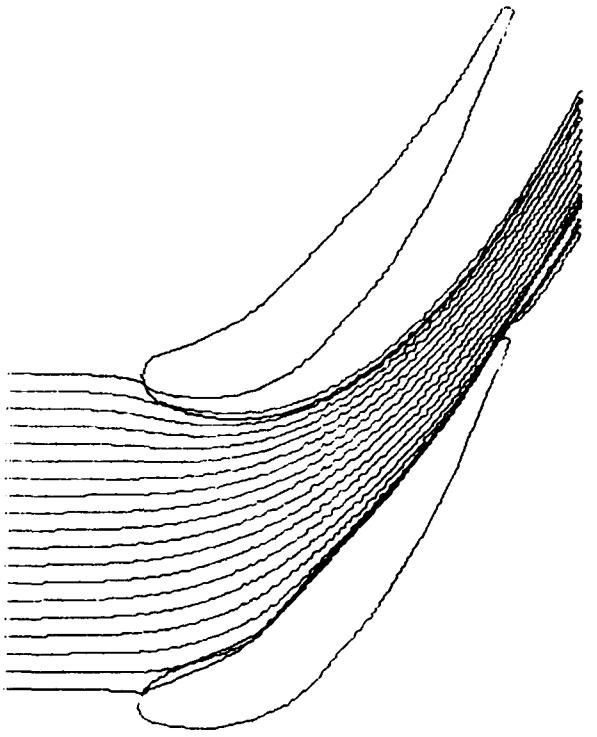

FIG. C-2. STATOR - BLADE EXIT ANGLE REDUCED 2.5°, PARTICLE TRAJECTORIES

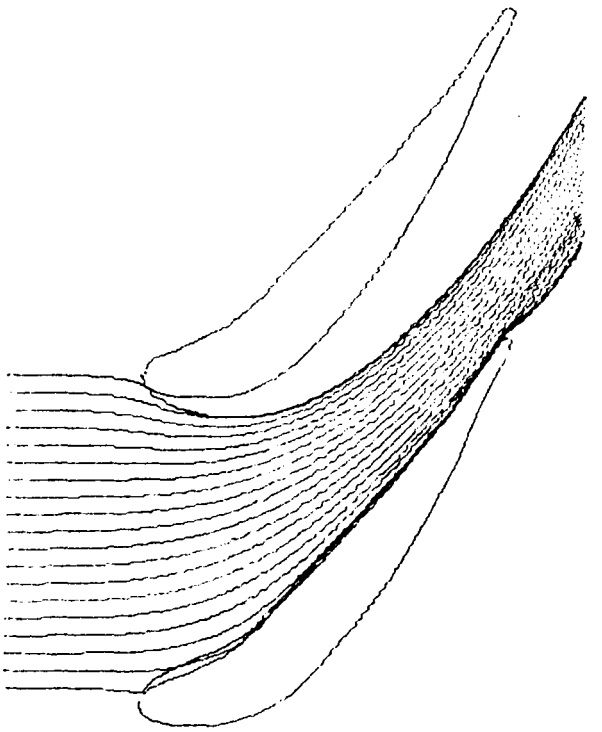

FIG. C-3. STATOR - BLADE EXIT ANGLE REDUCED 5.0°, PARTICLE TRAJECTORIES

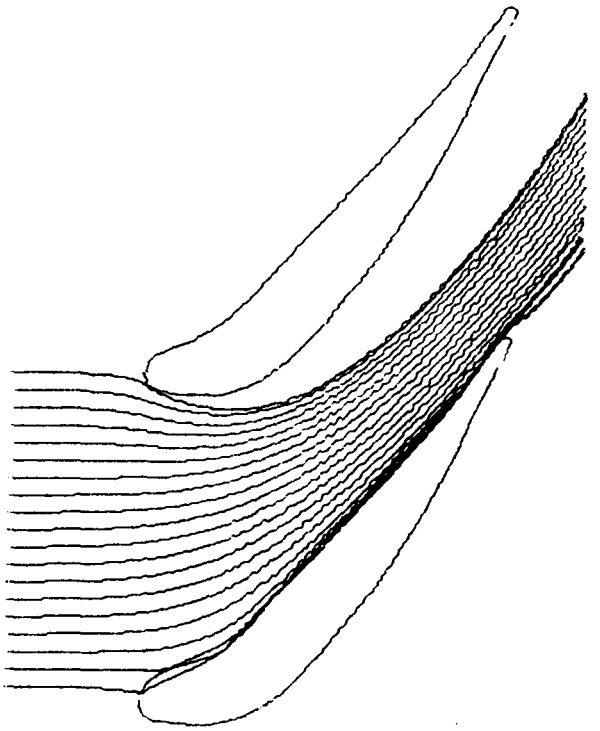

FIG. C-4. STATOR - BLADE EXIT ANGLE REDUCED 7.5°, PARTICLE TRAJECTORIES

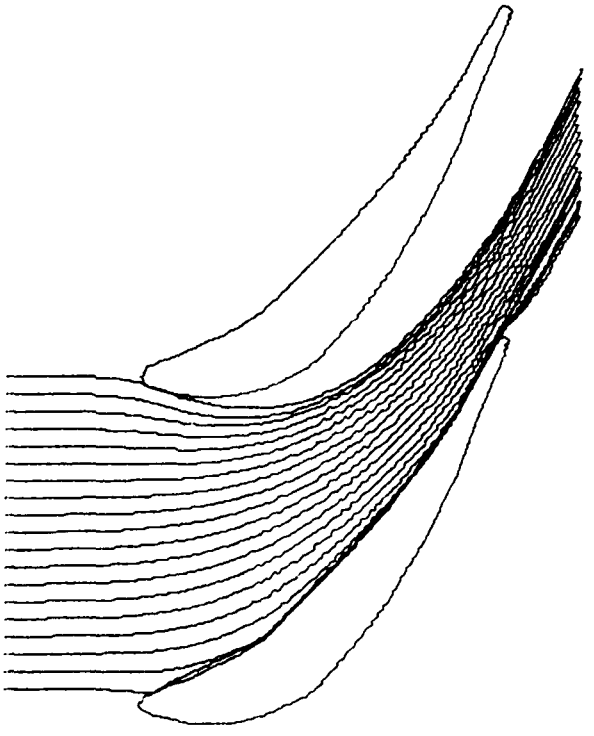

FIG. C-5. STATOR - LEADING EDGE RADIUS = ½ R_1, PARTICLE TRAJECTORIES

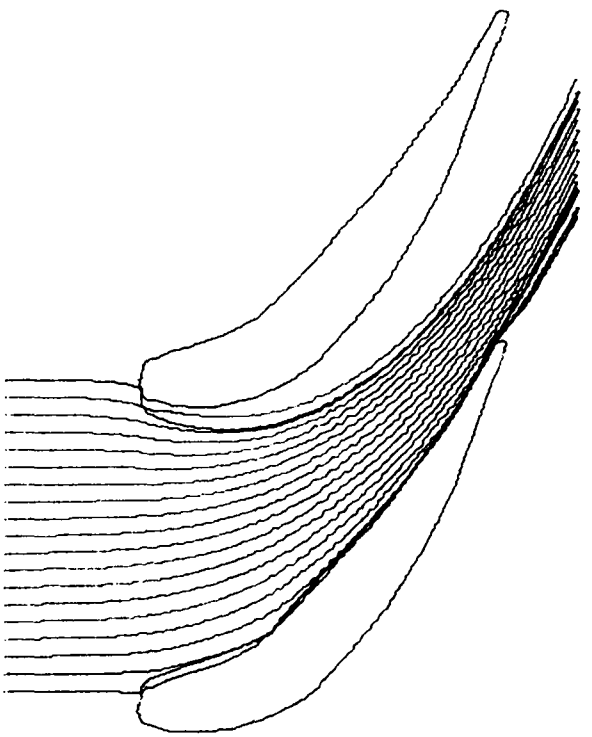

FIG. C-6. STATOR - LEADING EDGE RADIUS = 1.67 R_1, PARTICLE TRAJECTORIES

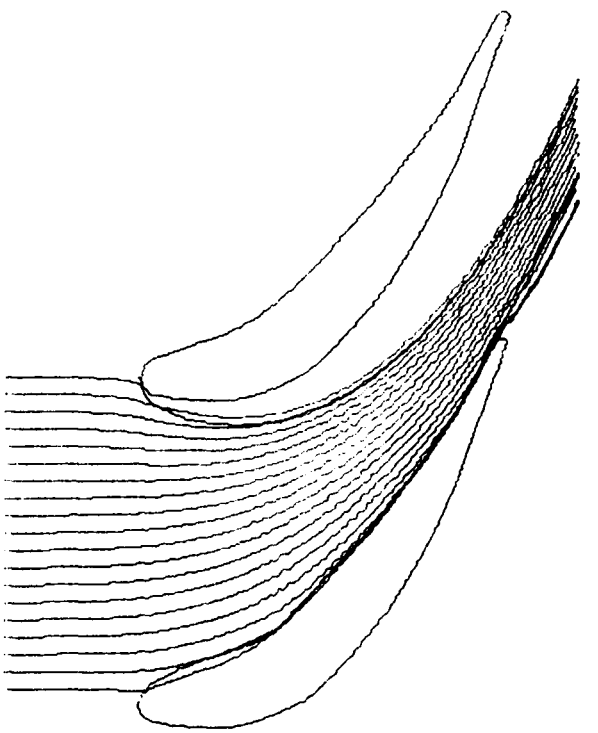

FIG. C-7. STATOR - $\Lambda = 0$, PARTICLE TRAJECTORIES

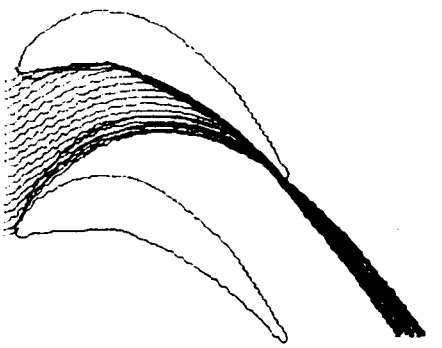

FIG. C-8. WESTINGHOUSE ROTOR, PARTICLE TRAJECTORIES

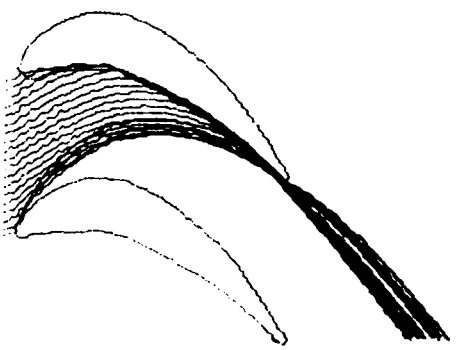

FIG. C-9. ROTOR - BLADE EXIT ANGLE REDUCED 2.5°, PARTICLE TRAJECTORIES

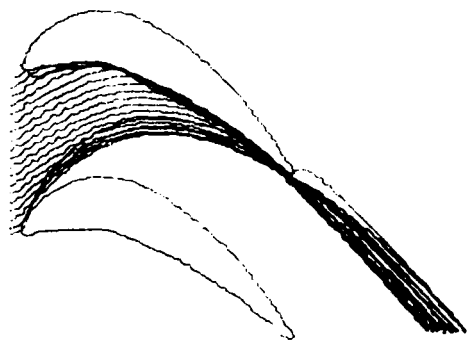

FIG. C-10. ROTOR - BLADE EXIT ANGLE REDUCED 5.0°, PARTICLE TRAJECTORIES

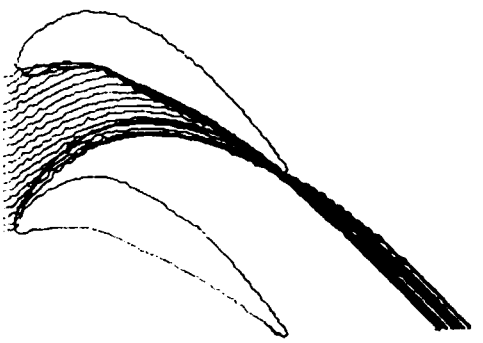

FIG. C-11. ROTOR - BLADE EXIT ANGLE REDUCED 7.5^{o}, PARTICLE TRAJECTORIES

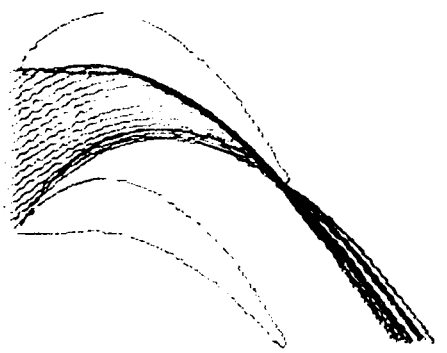

FIG. C-12. ROTOR - LEADING EDGE RADIUS = ¼ R_2, PARTICLE TRAJECTORIES

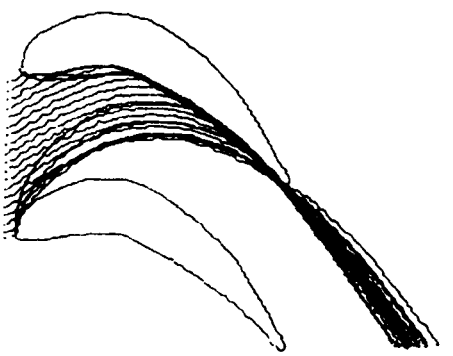

FIG. C-13. ROTOR - LEADING EDGE RADIUS = 3 R_2, PARTICLE TRAJECTORIES

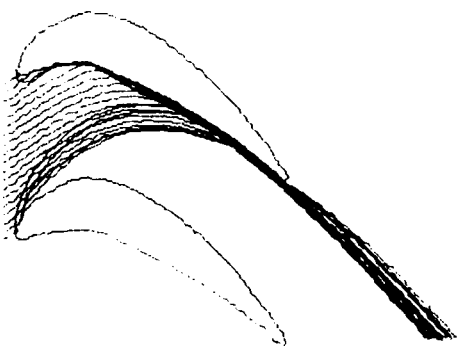

FIG. C-14. ROTOR - $\Lambda = 0$, PARTICLE TRAJECTORIES

The vita has been removed from the scanned document

AN ANALYTICAL INVESTIGATION OF THE EFFECT
OF BLADE PROFILE VARIATIONS ON THE EROSION
OF COAL-FIRED TURBINE BLADES

by

Jack Allan Kinback

(ABSTRACT)

The effect of blade profile variations on the erosion of turbine blades subjected to flow containing particulates was analytically determined. To accomplish this end, the two-dimensional inviscid main flow field was determined for each blade passage. A semi-empirical model of erosion was combined with available experimental data to predict erosion on the blade surfaces.

Maximum erosion was found to be at the trailing edge of the stator and rotor and at the leading edge of the rotor. The trailing edge erosion of the stator and rotor was decreased as the blade exit angle was decreased. The trailing edge erosion of the stator and rotor was also decreased when the blade leading edge radius was reduced.

Reducing the degree of reaction of the turbine stage caused a change in distribution of erosion levels along the blade surface.